Delft University of Technology

Document Version
Final published version

Licence
CC BY

Citation (APA)
Do Minh, H., Perez, G. A. C., Barreto, W., & Zevenbergen, C. (2026). Spatiotemporal urban flood expansion and propagation by the percentage of nodes in flood assessment (PNFA). *Hydrology Research*, *57*(3), 383-406. https://doi.org/10.2166/nh.2026.046

Important note
To cite this publication, please use the final published version (if applicable).
Please check the document version above.

Copyright
In case the licence states “Dutch Copyright Act (Article 25fa)”, this publication was made available Green Open Access via the TU Delft Institutional Repository pursuant to Dutch Copyright Act (Article 25fa, the Taverne amendment). This provision does not affect copyright ownership.
Unless copyright is transferred by contract or statute, it remains with the copyright holder.

Sharing and reuse
Other than for strictly personal use, it is not permitted to download, forward or distribute the text or part of it, without the consent of the author(s) and/or copyright holder(s), unless the work is under an open content license such as Creative Commons.

Takedown policy
Please contact us and provide details if you believe this document breaches copyrights.
We will remove access to the work immediately and investigate your claim.

This work is downloaded from Delft University of Technology.

Hydrology Research

© 2026 The Authors

Hydrology Research Vol 57 No 3, 383 doi: 10.2166/nh.2026.046

Spatiotemporal urban flood expansion and propagation by the percentage of nodes in flood assessment (PNFA)

Ha Do Minh [a,b,c,*], Gerald Augusto Corzo Perez [a,b], Wilmer Barreto [d] and Chris Zevenbergen [a,b]

[a] IHE Delft Institute for Water Education, Westvest 7, 2611 AX Delft, Netherlands
[b] Faculty of Civil Engineering and Geosciences, Delft University of Technology (TU Delft), Stevinweg 1, 2628 CN Delft, The Netherlands
[c] Faculty of Infrastructure and Environment Engineering, Ha Noi Architectural University, Km 10, Nguyen Trai, 11400 Thanh Xuan, Ha Noi, Viet Nam
[d] Department of Civil Engineering and Geology, Catholic University of Temuco, Manuel Montt 056, La Araucanía, Chile
*Corresponding author. E-mail: h.do@un-ihe.org

HDM, 0000-0002-7270-5611; GACP, 0000-0002-2773-7817; WB, 0000-0002-1861-0742; CZ, 0000-0002-9359-1625

ABSTRACT

Urban pluvial flooding is influenced by rainfall intensity, drainage capacity, and urban infrastructure. While prior studies mapped flood extents, the spatiotemporal dynamics of drainage saturation and overflow remain underexplored. This study introduces the percentage of node in flood assessment (PNFA) and flood expansion rate (FER) to quantify flood spread within drainage networks. Using EPA SWMM, three historical storms (2008, 2019, and 2020) and seven return-period scenarios were simulated in Do Lo, Hanoi, Vietnam. The results show that despite rainfall variability, spatiotemporal flood patterns remain stable, indicating predictable propagation pathways. FER values ranged from 0.17 (slow) to 0.902 (rapid), reflecting flood expansion speed under light to heavy rainfall. Spatiotemporal analysis produced hazard maps, capturing both spatial and temporal dimensions, revealing not only a persistent critical hotspot near AH13 but also consistent flood evolution patterns across various scenarios. These findings shift perspectives on flood preparedness by emphasizing timing, sequence, and hotspot stability. This study advances urban flood risk assessment through spatiotemporal hazard mapping, offering insights essential for mitigation, urban planning, and drainage resilience. Incorporating time-sensitive models is crucial for managing flood risks amid increasing extreme weather events.

Key words: physics-based model, pluvial flood, spatiotemporal flood, urban flood modelling, urban flood response

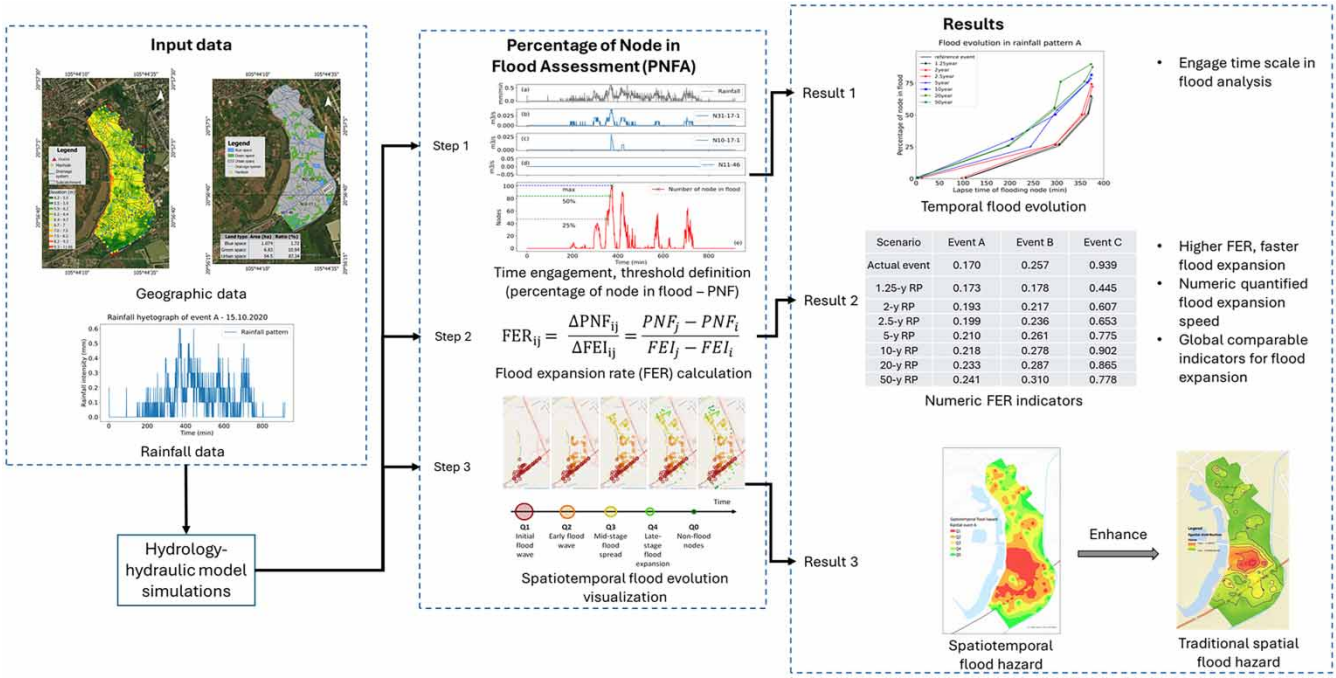
HIGHLIGHTS

- PNFA combines temporal and spatial analyses for urban flood assessments.
- Five quartiles capture flood evolution throughout the flooding timeline.
- FER quantifies flood agility, ranging from 0.17 (low) to 0.902 (high).
- Spatiotemporal flood evolution stabilized across varying rainfall scenarios.
- Spatiotemporal hazard maps, showing a critical hotspot near AH13, improve traditional spatial ones.

This is an Open Access article distributed under the terms of the Creative Commons Attribution Licence (CC BY 4.0), which permits copying, adaptation and redistribution, provided the original work is properly cited (http://creativecommons.org/licenses/by/4.0/).

Downloaded from iwaponline.com/hr/article-pdf/57/3/383/1608758/nh2026046.pdf
by Delft University of Technology user

GRAPHICAL ABSTRACT



Scenario	Event A	Event B	Event C
Actual event	0.170	0.257	0.939
1.25-y RP	0.173	0.178	0.445
2-y RP	0.193	0.217	0.607
2.5-y RP	0.199	0.236	0.653
5-y RP	0.210	0.261	0.775
10-y RP	0.218	0.278	0.902
20-y RP	0.233	0.287	0.865
50-y RP	0.241	0.310	0.778

INTRODUCTION

Urban flooding, defined as water-related hazards in densely populated and vulnerable areas (Alves *et al.* 2024), remains a critical challenge for cities worldwide (Angelakis *et al.* 2023). With 60% of the global population residing in urban areas, floods pose severe physical, psychological, and health risks (Tellman *et al.* 2021; Abass *et al.* 2022). Contaminated flood-waters, often a mix of stormwater and sewage, increase the prevalence of waterborne diseases (Nguyen *et al.* 2017; Huynh *et al.* 2019; Olsson 2019; Beg *et al.* 2020). Although mortality rates have declined, floods remain among the deadliest natural hazards, causing over 5,500 deaths globally in 2024 (Jonkman *et al.* 2024; CRED 2025). Beyond public health, floods inflict extensive damage on infrastructure, including transportation networks and critical facilities (Chen *et al.* 2015; Lu *et al.* 2023; Amornsiripanitch *et al.* 2025; Paulik *et al.* 2025; Schaum *et al.* 2025).

Rapid urbanization, through increased impervious surfaces, disrupts natural hydrological processes and amplifies runoff, while climate change intensifies rainfall frequency and magnitude, further exacerbating flood risk (Miller & Hutchins 2017; Yang *et al.* 2021; Rogers *et al.* 2025). Unlike fluvial floods, which can be mitigated through structural measures such as dikes, pluvial floods – triggered by intense urban rainfall – are highly localized and difficult to predict. Despite generally causing less severe damage, their higher frequency results in annual economic losses than fluvial floods (Tanaka *et al.* 2020).

Flood risk management strategies range from structural interventions to land-use planning, early warning systems, emergency response, and integrated approaches (Genovese & Thaler 2020). However, the complexity of urban drainage networks complicates spatiotemporal flood modelling (Francipane *et al.* 2021). Moreover, characterized by rapid onset and short duration, flash flood increases regularly both in frequency and intensity under the climate change effects, leaving limited time for response (Acosta-Coll *et al.* 2018; Al-Rawas *et al.* 2024; Sadkou *et al.* 2024). Rainfall heterogeneity strongly influences flood dynamics, while drainage system variability and storm distribution alter flood pathways and intensity (Leandro *et al.* 2016; Prokić *et al.* 2019). Current flood risk assessments primarily emphasize spatial distribution, often neglecting the temporal dynamics of flood evolution. This limitation reduces their effectiveness in supporting timely decision-making for evacuation and resource allocation. Existing methods rarely quantify flood propagation speed or visualize flood expansion over time, leaving a critical gap in understanding spatiotemporal flood behaviour (Rosenzweig *et al.* 2018; Mishra *et al.* 2022).

This research aims to develop an innovative protocol, the percentage of node in flood assessment (PNFA), to integrate temporal flood evolution into flood hazard analysis and visualization. PNFA introduces a novel indicator, the flood expansion rate (FER), to quantify flood spreading speed across space and time. A case study, Do Lo, Yen Nghia Precinct, Ha Dong

Downloaded from iwaponline.com/hr/article-pdf/57/3/383/1608758/nh2026046.pdf
by Delft University of Technology user

District, Hanoi, Vietnam, was chosen to represent the PNFA application under 24 rainfall scenarios, producing spatiotemporal hazard maps that capture both flood extent and timing.

The main contributions of this study are (1) developing a new spatiotemporal flood assessment framework, PNFA, that incorporates temporal dynamics into flood hazard mapping; (2) Introduction of the FER as an indicator for quantifying flood propagation speed; and (3) showing the application and validation of PNFA in an urban case study, demonstrating its potential for enhancing flood preparedness and emergency response planning. The remainder of this paper is structured as follows: Section 'Background' reviews the background and research gaps; Section 'Study area' gives the overall information of the research area; Section 'Materials and methods' describes the details of the data and methodology, including PNFA; Section 'Results' explains the application results; Section 'Discussion' discusses the findings, limitations, and future works, and concludes with the final 'Conclusion' section.

BACKGROUND

Flood modelling is a critical component of urban flood mitigation strategies, enabling the simulation and visualization of flood dynamics. Conceptually, physically based models are widely employed to characterize urban flood behaviour (Getirana *et al.* 2023; Lameche *et al.* 2023; Hauser *et al.* 2024; Sañudo *et al.* 2024). These models typically focus on two key aspects: (1) identifying saturation points within a drainage infrastructure, such as manholes, and (2) representing the flow dynamics of water and its interaction with surface runoff. The integration of one-dimensional (1D) and two-dimensional (2D) hydrodynamic models facilitates a more comprehensive understanding of urban flood processes (Leandro *et al.* 2009; Seyoum *et al.* 2012; Cea *et al.* 2025). Urban flood management efforts predominantly concentrate on drainage systems, which constitute the primary engineered infrastructure for flood control. Among the various physics-based models available – such as HEC-RAS, HEC-HMS, SWMM, and PCSWMM – the EPA Storm Water Management Model (SWMM) is frequently utilized due to its simplicity, open-source accessibility, and rapid computational performance (Piadeh *et al.* 2022; Snikitha *et al.* 2025). These models, grounded in physical hydrological processes, have the potential to provide direct insights into flood event locations and timings. However, recent research has largely focused on static flood scenarios, with limited attention to the temporal evolution of flood events. In parallel, hybrid artificial intelligence (AI) models – integrating hydrological modelling with machine learning and deep learning techniques – have emerged as powerful tools for flood prediction. These models enhance predictive capabilities by imputing missing data, improving calibration procedures, and generating flood risk maps (Bentivoglio *et al.* 2023; Berkhahn & Neuweiler 2024; Qin *et al.* 2024; Schmid & Leandro 2024; Zeng *et al.* 2025; Zhou *et al.* 2025). Despite their flexibility and robustness, data-driven models have primarily focused on static representations of flood risk. The absence of standardized methodologies for incorporating temporal dynamics into flood assessments remains a significant limitation, hindering the visualization of spatiotemporal flood evolution.

Incorporating both spatial and temporal dynamics into flood risk assessment is essential for improving hazard analysis and emergency response strategies. Understanding drainage saturation points and the onset of flooding is fundamental for accurate flood risk assessment, as demonstrated in the previous studies (Mishra *et al.* 2020; Afsari *et al.* 2022; Levin & Phinn 2022; Zhou *et al.* 2022; Wijaya *et al.* 2023). This information not only identifies flood-prone areas but also supports effective flood risk mapping. However, flood risk assessments have traditionally relied on static representations, often neglecting the dynamic nature of floods in hazard analysis (Arrighi *et al.* 2017; Dong *et al.* 2022; Li *et al.* 2023). Sequential saturation patterns and variations in water volume across urban areas are critical for evaluating hazard levels, particularly given the potential for floodwaters to exert forces capable of moving individuals or vehicles. Even relatively shallow floods can have severe consequences due to their kinetic energy (Zhu *et al.* 2023). Moreover, a timely response is another key factor in reducing flood-related damages. In the case of flash floods, which develop rapidly under intense rainfall, a delayed action can lead to severe consequences (Archer & Fowler 2018). Early warning systems have, therefore, become essential in non-structural flood management measures. Real-time forecasting enables decision-makers to anticipate disaster scenarios and implement emergency response plans proactively (Henonin *et al.* 2013; Mahiddin *et al.* 2023). Time-sensitive communication is critical for the effectiveness of flood warnings (Kuller *et al.* 2021; Fernández-Nóvoa *et al.* 2024). Consequently, flood risk assessments must incorporate both spatial and temporal dimensions to provide comprehensive information for management tools such as hazard maps (Wang *et al.* 2022; Corzo Perez *et al.* 2024). This underscores the need to study flood dynamics, including initiation timing, propagation speed, and spatiotemporal saturation patterns within drainage networks.

Downloaded from iwaponline.com/hr/article-pdf/57/3/383/1608758/nh2026046.pdf
by Delft University of Technology user

Flood risk assessments have traditionally relied on static representations, overlooking the dynamic nature of flood evolution and its implications for hazard analysis and emergency response. Historically, spatiotemporal flood analysis has focused on long-term and large-scale patterns, typically at annual or decadal scales. Examples include global flood classifications from 1985 to 2019 (Liu *et al.* 2022), continental flood extent trends over 70 years in Europe (Fang *et al.* 2024), and national-scale exposure patterns in the United States (Abedin *et al.* 2024). Regional studies have also examined the influence of land use and land cover changes on flood behaviour over multiple decades, such as in Bangkok (Darnkachatarn & Kajitani 2024). While these studies provide valuable insights into long-term exposure trends, they offer a limited understanding of short-term flood dynamics during individual events.

Recent research has shifted towards event-scale spatiotemporal analysis. Spatiotemporal rainfall distribution has been shown to significantly influence both surface and subsurface flood responses (Zhou *et al.* 2021) and trigger pressurized flows and geyser-like eruptions in urban drainage systems (Vasconcelos *et al.* 2024). Induced rainfall, identified as the primary driver of urban pluvial flooding, was classified spatiotemporally using the K-shape clustering algorithm. The temporal evolution of rainfall patterns was incorporated into the categorization process. However, this study focused exclusively on induced rainfall, and a comprehensive flood impact assessment has not yet been conducted (Qiu *et al.* 2025). Spatiotemporal flood hazard was initially analysed based on the combination flood result of traditional modelling (SWMM) and machine learning (NARX). Flood locations and timing were predicted and interpolated to a 2D map, which is the foundation for evacuation route prediction. Although flood evolution was presented in hourly flooding time steps, the temporal flood distribution was presented in a sequence of spatial flood maps (Lee *et al.* 2020). In the built environment, a time-dependent model was introduced for flood risk assessment, incorporating user characteristics. Flood risk was assessed and calculated for each categorized group based on individuals' vertical position within the building and their home presence duration. Flood evacuation routes, as a result, were designed based on spatiotemporal flood risk analysis (Bernardini *et al.* 2024). As the underground spaces of buildings are vulnerable to flood, time is an important factor affecting flood risk and escape routes, besides flood prevention measures. 2D flow simulations were performed to consider the inflow of rainfall, and water shield designs (Shin *et al.* 2021). The spatiotemporal impacts of flooding on the urban metro system in Hong Kong were evaluated using a two-dimensional shallow water equations (2D SWE) model to simulate flood events. Temporal flood dynamics were successfully integrated into the analysis and translated into flood risk assessments for the metro network, enabling the identification of high-risk metro station locations (Liang *et al.* 2026). The spatiotemporal dynamics of flooding were examined to establish a foundational framework for analysing cascading failures within critical infrastructure systems. The spatial and temporal impacts of flood events on interdependent infrastructure networks were effectively represented, and the temporal progression of these impacts was clearly demonstrated (Wang *et al.* 2025). A comparative analysis of spatiotemporal pluvial flood predictions generated by a physics-based model and a hybrid deep learning approach demonstrated effective temporal representation of flood dynamics. Predictions produced using a convolutional neural network (CNN) were closely aligned with those obtained from the CADDIES model, highlighting the potential of deep learning techniques for spatiotemporal flood forecasting (Woo *et al.* 2025). Similarly, a comparative analysis of spatiotemporal flood predictions was conducted between a physics-based model (MIKE PLUS) and a U-shaped recurrent neural network (U-RNN), demonstrating the competitive potential of deep learning approaches for pluvial flood forecasting (Cao *et al.* 2025). In those studies, although the temporal flood dynamics were successfully integrated into the analysis, the temporal flood evolutions were still represented by a sequence of flood risk maps. The explicit representation of temporal flood propagation processes remains absent. The absence of consistent frameworks and protocols for representing spatiotemporal flood dynamics remains a major limitation, constraining both predictive accuracy and the design of adaptive flood management strategies.

STUDY AREA

The study area, Do Lo, is located in the southwest of Yen Nghia Ward, Ha Dong District, the fringe of Ha Noi City, Viet Nam (Figure 1(a)). This urban area was transformed from two old villages, as decided by the Government (Vietnam Government 2006, 2008). A total of 10,373 residents were living in this 61.5 ha area in 2019 (Yen Nghia Comune People's Committee 2019). Do Lo, Yen Nghia, is a dense urbanized area with a population density of approximately 16,900 persons/km^2.

The case study has a tropical and monsoonal climate with four distinct seasons (i.e. spring, summer, autumn, and winter). Average temperature is +23 °C, ranging from + 5 to +38 °C. The rainy season (from May to October) coincides with the Asian monsoon (Ho *et al.* 2011).

Downloaded from iwaponline.com/hr/article-pdf/57/3/383/1608758/nh2026046.pdf
by Delft University of Technology user

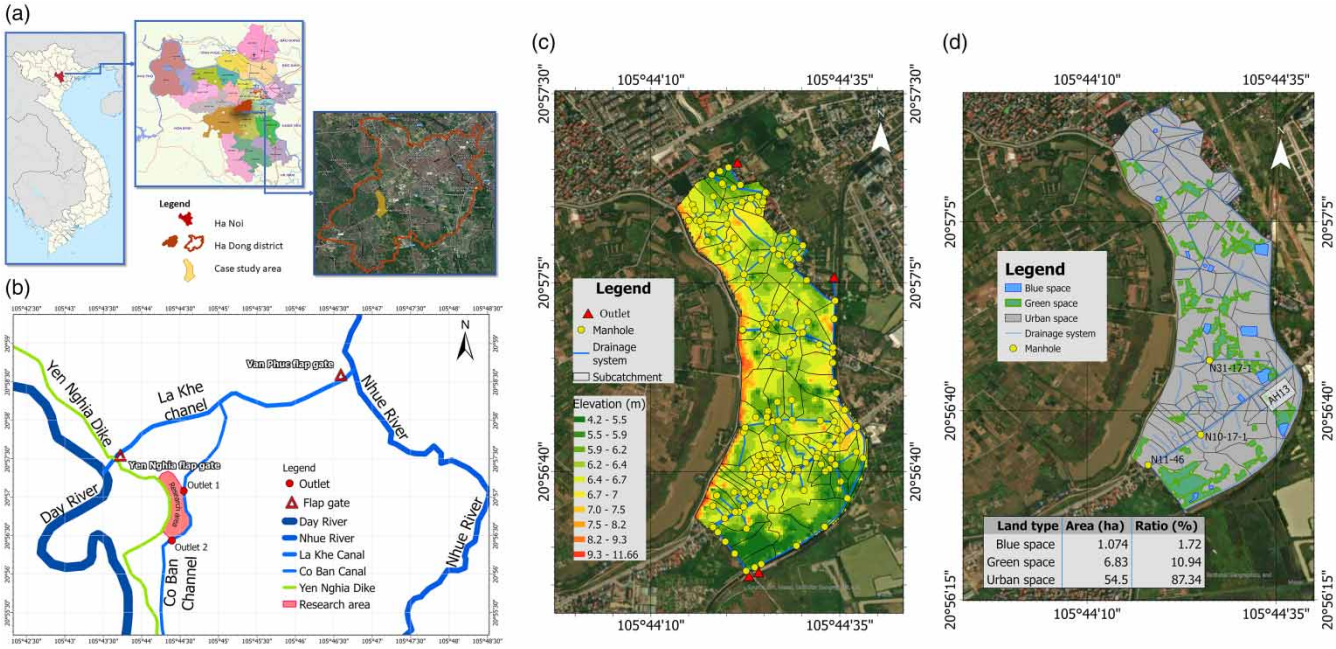


Figure 1 | Case study details: (a) Location; (b) connections with the local hydrological system; (c) digital elevation model (DEM), subcatchments, and the drainage system; and (d) land use and land cover (updated from previous research (Do Minh *et al.* 2023)).

Do Lo is positioned in the Red River Delta; therefore, this place has flat topography with an average elevation of 5 m. Although located between two rivers (i.e. the Day River and the Nhue River), this area is protected from fluvial flood thanks to dike systems along these two rivers. The La Khe canal connects these two rivers by the Yen Nghia Gate (west side) and the Van Phuc Gate (east side). Yen Nghia pumping station, located at the Yen Nghia gate, pumps water from the La Khe canal to the Day River. Co Ban Chanel plays an important role in conveying the rainwater and wastewater from the research area to the La Khe canal. Rainwater and domestic wastewater are collected by a combined sewer system (CSS) throughout the research area before discharge into the Co Ban canal via southern and western outfalls (Figure 1(b)). The water level in the Co Ban canal is under control and regulated at 5.12 m (assuming stable).

The main road, Asian Highway 13 (AH13) passes through the case study area (Figure 1(c)). During rush hour, this main road has approximately 6,000 vehicles per hour travelling through. However, pluvial floods are detected frequently on this main road, constraining the traffic flux, according to the Ha Noi Sewage and Drainage system Company (HSDC) report.

Situated on the outskirts of Ha Noi city, Do Lo District has witnessed rapid urbanization driven by the city's expansion. Nonetheless, the area has received limited financial support, particularly for infrastructure development, since it is often left out in urban planning projects (Luo *et al.* 2018). As a result, the existing drainage system has struggled to keep pace with the speed of urbanization. Additionally, projections indicate an anticipated increase in extreme rainfall events because of climate change (Tran-Anh & Ngo-Duc 2024). Companies that have responsibilities for flood risk management (e.g. Hanoi Drainage and Sewage system Company) are struggling to manage flood risks in this area due to the rapid occurrence of pluvial flooding and limited human resources.

MATERIALS AND METHODS

Data sources

The data used in this research were collected from several sources. To construct the framework of the drainage system model, data on the digital elevation map (DEM). Drainage system and land cover were collected from Ha Noi Urban Planning Institute (HUPI), Ha Noi Sewage and Drainage system Company (HSDC), and open-source Google Earth Pro, respectively. To generate the rainfall scenarios, rainfall distributions were mainly obtained from HSDC. A historical rainfall event and a 47-year daily rainfall dataset from 1974 to 2020 were acquired from the Viet Nam National Centre for Hydrometeorological Forecasting (NCHMF). To evaluate fluctuations in domestic wastewater discharge, daily water supply data from January 2021

Downloaded from iwaponline.com/hr/article-pdf/57/3/383/1608758/nh2026046.pdf
by Delft University of Technology user

were obtained for research from the Ha Dong Water Supply Company (HADOWA). Additionally, flood extents during the rainfall events were achieved through flood data collection campaigns, which were specially organized in collaboration with citizens of the research area.

Research method

This study followed a systematic approach comprising five phases: (1) drainage network model development, (2) calibration and validation, (3) scenario estimation, (4) simulation, and (5) spatiotemporal analysis (Figure 2). The drainage model was constructed using hydraulic data from local stakeholders, including DEM, drainage system layout, land cover, subcatchments, and dry-weather conditions. Calibration and validation employed field data on flood extent, water levels, and rainfall intensity collected during campaigns in 2019 and 2020. Scenario estimation was based on the statistical analysis of a 47-year rainfall record (1974–2020) and three observed storms (2008, 2019, and 2020). Flood simulations were performed using SWMM, and outputs were analysed using spatiotemporal metrics to assess flood patterns, dynamics, and propagation velocity. To quantify these changes, the FER was introduced. Subsequent sections detail each step.

Step 1: hydrology-hydraulic model build-up

Model set-up. To analyse urban flood responses to storm events, a detailed drainage network model was developed. Pre-processed inputs included DEM, drainage system data, land use and land cover, boundary conditions, and dry-weather flow (Figure 1). Using the 1D SWMM, the model focused on the underground drainage system as the primary determinant of flood locations. Subcatchments were delineated from the existing maps, with land cover data distinguishing pervious and impervious areas. Key nodes represented subcatchment outlets and conduit junctions, each assigned a 40 m^2 ponding area. Boundary conditions were defined by the Co Ban channel at the eastern district, with a fixed outfall water level of 5.12 m.

Urban catchment delineation. A total of 114 subcatchments were delineated based on DEM, drainage networks, and street pathways. The DEM, sourced from HUPI at a 20 m resolution, was fundamental for model set-up and originally referenced to

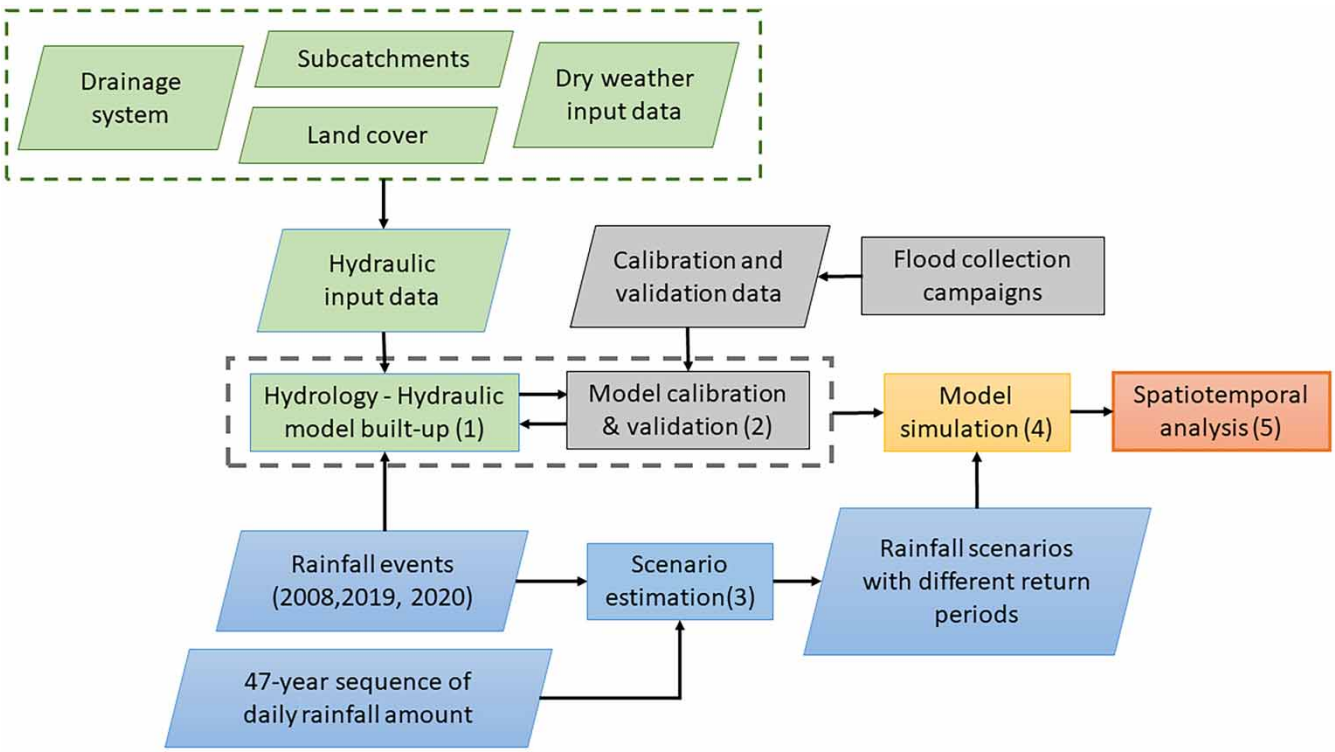


Figure 2 | Research scheme.

Downloaded from iwaponline.com/hr/article-pdf/57/3/383/1608758/nh2026046.pdf
by Delft University of Technology user

the VN2000 national coordinate system, later converted to WGS84 for data consistency (Pham Thi *et al.* 2019). Combined with street and drainage data, the DEM provided essential topographic information for accurate hydraulic modelling and flood simulation (Figure 1(c)).

Land cover. Land cover was classified into three categories: (1) blue space, including ponds and surface water, (2) green space, comprising vegetation, and (3) urban space, representing impervious surfaces. Do Lo is a highly urbanized area, with concrete surfaces covering 87.34%, while green and blue spaces account for 10.94 and 1.72%, respectively. The land cover map was manually compiled from LANDSAT imagery using Google Earth Pro (Figure 1(d)).

Estimation of domestic wastewater discharge. Dry-weather flow (DWF) was incorporated into the model to account for domestic wastewater contributions. Given the high urbanization of the area, 80% of the water supply was assumed to convert to wastewater, with daily consumption estimated at 300 litres per capita based on the Vietnamese standard TCXDVN 33:2006 (Ministry of Construction of Viet Nam 2006). Hourly fluctuations in water use were derived from consumption data collected in January 2021 and expert input from HADOWA-Ha Dong water supply company, ensuring realistic temporal variability. Daily wastewater discharge mirrored the water consumption pattern, providing hourly coefficients for more accurate modelling. So, the amount of domestic wastewater and its daily fluctuation can be defined for an individual. Wastewater discharge was assumed to originate solely from urban areas, while green and blue spaces contributed no polluted flow. DWF for each subcatchment was calculated as the product of per capita wastewater discharge, urban population density, and urban area.

Step 2: model calibration and validation

To simulate flood scenarios, five 24-h rainfall events (Events A–E) were selected (Table 1). Events A, B, and C were used for model calibration, while Events D and E served for validation. Four events (A, B, D, and E) were obtained from HSDC, recorded near the study area at 1-min intervals on 15 October 2020, 29 August 2019, 5 July 2022, and 11 August 2022. Event C, a historical storm that caused severe losses in Hanoi in 2008 (Luo *et al.* 2018), was included for its significance; its heaviest rainfall day (31 October 2008) was extracted at 1-h intervals from NCHMF.

Flood extent data were essential for model calibration and validation. Data collection campaigns were conducted during Events A, D, and E, involving both research teams and local residents. Calibration combined theoretical and empirical approaches with expert input, focusing on parameters, such as Manning's roughness coefficients for surfaces and pipes, and infiltration rates. This process followed a trial-and-error method consistent with previous studies and local recommendations. For validation, flood scenarios from Events D and E were simulated and compared against observed flood extents from the campaigns.

Step 3: rainfall scenario estimation

Rainfall scenarios for future flood prediction were developed using rainfall frequency analysis based on the annual maximum method. A 47-year daily rainfall dataset (1974–2020) from NCHMF was analysed following five steps (Figure 3(a)): (1) selecting annual maxima, (2) estimating exceedance probability using the Weibull method, (3) fitting the dataset to a log-Pearson III distribution as recommended by the U.S. Water Resources Council (England *et al.* 2019), (4) determining 24-h rainfall depths, and (5) extrapolating rainfall patterns into scenarios. Monte Carlo simulation was applied for seven return periods

Table 1 | Five actual precipitation events in 2008, 2019, 2020, and 2022

Rainfall event	Date of collection	Total rainfall amount (mm)	Usage	Resources	Resolution intervals	Equal returned period (years)
A	15.10.2020	84.8	Input	HSDC	1 min	1.25
B	29.8.2019	176.6	Input	HSDC	1 min	5
C	31.10.2008	565.9	Input	NCHMF	1 h	300
D	5.7.2022	117	Validation	HSDC	1 min	2
E	11.8.2022	219.7	Validation	HSDC	1 min	10

Downloaded from iwaponline.com/hr/article-pdf/57/3/383/1608758/nh2026046.pdf
by Delft University of Technology user

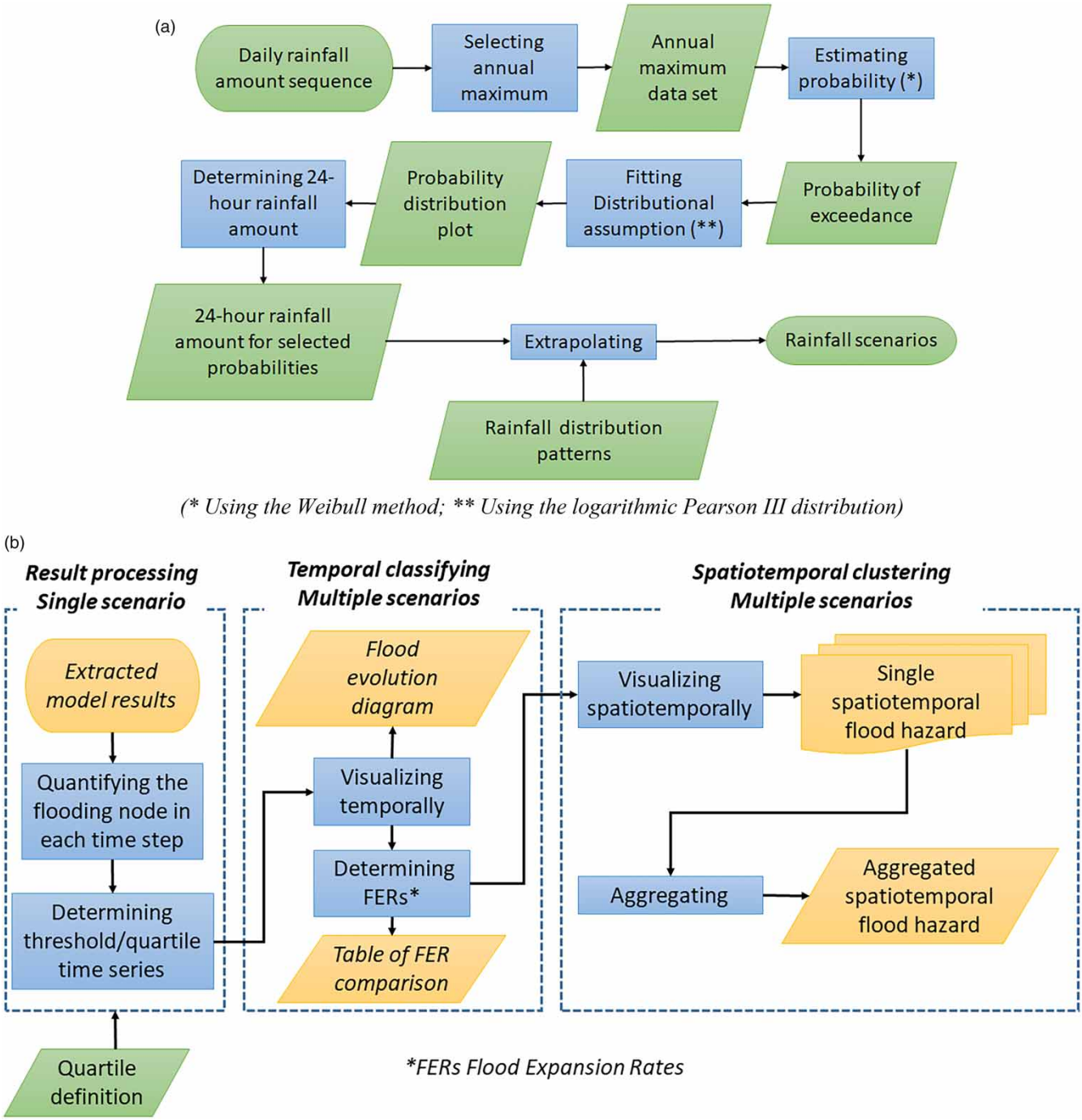


Figure 3 | Detailed methodologies of (a) rainfall frequency analysis and (b) PNFA.

(1.25, 2, 2.5, 5, 10, 20, and 50 years). Three rainfall patterns (A, B, and C) were derived from Events A, B, and C to represent temporal distribution characteristics.

Step 4: model simulation

A total of 24 rainfall scenarios were used for flood simulations: 21 synthetic scenarios generated by combining three rainfall patterns with seven return periods, and three observed events (A, B, C). Monte Carlo simulations were based on daily rainfall amounts, adjusting total volume while preserving hyetograph shape to maintain statistical reliability. However, this approach

Downloaded from iwaponline.com/hr/article-pdf/57/3/383/1608758/nh2026046.pdf
by Delft University of Technology user

may underrepresent short-duration peak intensities critical in extreme events. Flood simulations were performed in SWMM and processed using a custom Python script with the SWMM_api package (Pichler 2025). Although rainfall data covered 24 h, simulations spanned 72 h – 24 h before, during, and after the event – to stabilize domestic wastewater conditions and capture post-rainfall flooding.

Step 5: spatiotemporal analysis using the PNFA

Flood analysis was performed using simulation outputs from Step 4, integrating both spatial and temporal dimensions of flood hazards. Unlike conventional approaches focused solely on spatial distribution, this study employed the PNFA method to quantify flood risk across discrete time intervals based on node inundation thresholds. Key outputs included flood expansion rates, temporal flood progression patterns, and a spatiotemporal flood hazard map.

Percentage of node in flood assessment

The PNFA is a novel assessment approach for analysing urban flood dynamics over both space and time. PNFA concerns not only the spatial flood hazard but also the temporal flood hazard.

To incorporate the temporal scale into flood analysis, flooding time steps were thoroughly examined in each scenario before being aggregated to get a comprehensive analysis of the spatiotemporal flood evolution. The spatiotemporal flood evolution was presented in three forms: diagram expression (temporal flood expansion), numerical expression (FER), and map expression (spatiotemporal flood hazard maps). The spatiotemporal flood quartiles were defined to assist the temporal flood analysis. Figure 3(b) shows spatiotemporal flood analysis step by step: (1) flood result processing in a single scenario, (2) temporal classifying in multiple scenarios, and (3) spatiotemporal clustering in multiple scenarios.

Spatiotemporal flood quartile definition

To clarify the flood evolution spatiotemporally, flooded nodes were classified into four quartiles based on the flood sequence in time (Figure 4).

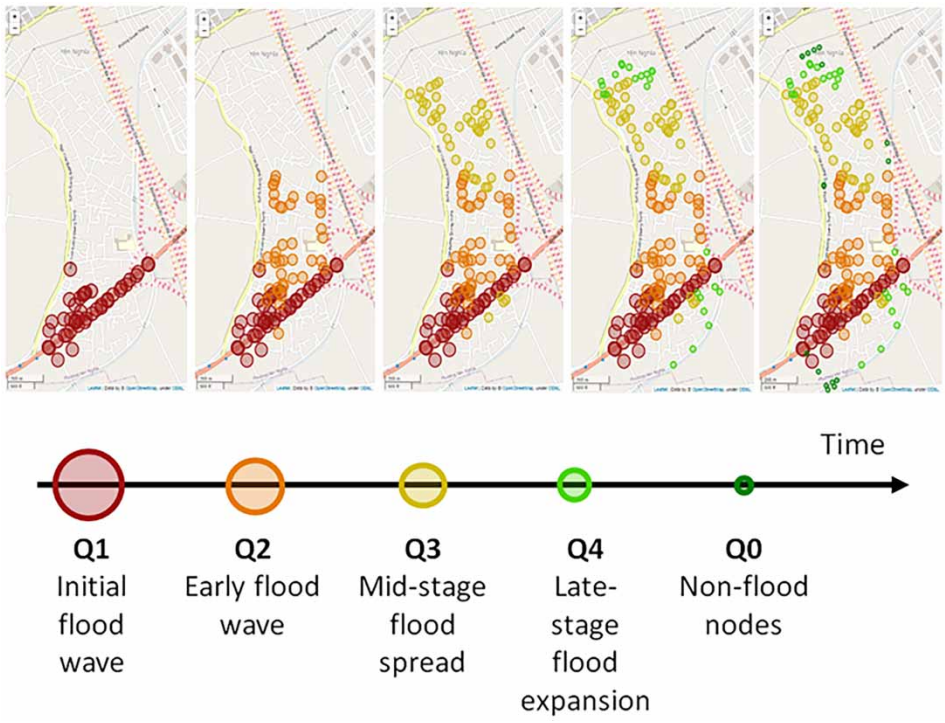


Figure 4 | Illustration of the flood evolution process during the flooding time.

Downloaded from iwaponline.com/hr/article-pdf/57/3/383/1608758/nh2026046.pdf
by Delft University of Technology user

These spatiotemporal quartiles were introduced in order to classify the magnitude of flood risk based on the time scale. These spatiotemporal quartiles included four main quartiles (i.e. Q1, Q2, Q3, Q4) and one extra quartile, Q0, for the non-flood manhole.

- Q1 (Initial flood wave): Represented the first quartile (0–25%) nodes in flood, encompassing the first 42 flooded nodes. This quarter captured the initial impact of the flood.
- Q2 (Early flood propagation): Constituted the second quartile (25–50%) nodes in flood, including flooded nodes from 43rd to 84th. These nodes flooded subsequently to the initial wave, marking the early stages of flood propagation.
- Q3 (Mid-stage flood spread): Encompassed the third quartile (50–75%) nodes in flood, from flooded nodes from 85th to 126th. This group indicated nodes that flooded during the mid-stage of the event.
- Q4 (Late-stage flood expansion): Included the final quartile (75–100%) nodes in flood, indicating the percentage of nodes that were the last ones experiencing the flood.
- Q0 (Non-flooded nodes): This category was reserved for nodes that did not experience a flood during the event, which were outside of the quartile classification.

Due to variations in scenario conditions, the distribution of nodes across these classifications could differ. In some scenarios, there were no nodes falling into the Q3 or Q4 categories. Those events might have more concentrated floods or just be less intensive flood events. Conversely, some other scenarios, with broader flood impacts, have nodes distributed across all four quartiles. Across the scenarios, several nodes that remained unaffected by flooding were consistently classified as Q0, providing a clear distinction between flooded and non-flooded regions within the model simulations. The flood with less than 25% of nodes in flood was not considered a critical condition.

This quartiles definition was an initial but essential step for spatiotemporal analysis, which gave thresholds to determine the flood propagation speed in a later phase.

Spatiotemporal analysis

The spatiotemporal analysis focused on both the temporal and spatial distributions of floods by three consecutive stages: result processing, temporal classification, and spatiotemporal clustering.

Firstly, result processing was applied for each scenario simulation to understand the flood situation at each time step. Flooding data were extracted from the simulation results. The number of flooding nodes in each time step was tracked. When the number of flooded nodes reached certain quartile thresholds, the time periods were recorded. Those incremental time series represent the flood evolution during the flooding time.

Secondly, temporal classifying focused only on the temporal scale of floods, assessing the agility and rapidity of the flood extension. Flood evolution time series of various scenarios were charted to illustrate the flood expansion speed. This expansion speed was also calculated numerically by FER.

Finally, spatiotemporal clustering provided a deeper analysis of the previous stage by considering both the temporal and spatial distribution of floods across all scenarios. Single spatiotemporal flood distributions were clustered and visualized geographically using prior classifications and key node locations. The aggregated spatiotemporal flood distribution was constructed by overlaying all single spatiotemporal flood distributions, providing a comprehensive view of spatiotemporal flood hazards. This analysis identified two key types: the most critical spatiotemporal flood hazard and the highest potential spatiotemporal hazard.

FER

In order to compare the flood agility and rapidity numerically during the temporal classification, FER was introduced in Formula (1):

$$\mathrm{FER}_{ij} = \frac{\Delta \mathrm{PNF}_{ij}}{\Delta \mathrm{FEI}_{ij}} = \frac{\mathrm{PNF}_j - \mathrm{PNF}_i}{\mathrm{FEI}_j - \mathrm{FEI}_i} \tag{1}$$

where i and j are the thresholds of the percentage of node in the flood the certain quartile (e.g. 25 and 50%). FER_{ij} is the flood expansion rate from threshold i to threshold j. FEI_{ij} is the flood evolution interval from threshold i to threshold j. PNF_{ij} is the percentage of node in the flood from threshold i to threshold j.

In this research, we considered threshold i at zero minutes when the induced rain started.

Downloaded from iwaponline.com/hr/article-pdf/57/3/383/1608758/nh2026046.pdf
by Delft University of Technology user

The percentage of node in the flood at moment j PNF_j is calculated by Formula (2):

$$PNF_j = \frac{NNF_j}{TN} \times 100 \quad (2)$$

where NNF is the number of nodes in the flood at threshold j. TN is the total number of nodes in the drainage system in the considered assessment.

RESULTS

Modelling results

Model calibration and validation

During the flood data collection campaigns, residents of AH13 were asked to report flood extents during Events A, D, and E. Flood extent data were gathered by both local citizens and workers living and working in the study area. The reported flood extents for Events A, D, and E closely matched the model results, indicating that the developed model effectively replicated the hydraulic system and flood conditions in the area (Figure 5).

Rainfall patterns and rainfall scenarios

Figure 6 represents five observed rainfall hyetographs (Events A–E). Events A, B, and C were used for model development and calibration, while Events D and E were used for validation. Temporal rainfall patterns (patterns A, B, and C) were derived from Events A–C and applied as baselines for scenario generation. Rainfall frequency analysis identified seven return periods, with corresponding daily rainfall depths, summarized in Table 2. Each pattern was scaled to these return periods, producing 21 scenarios. Temporal distributions remained unchanged, while intensities were adjusted. All scenarios were generated at 1-min and 1-h intervals.



Figure 5 | Flood extent in the model and in the field during Event D (a1, a2) and Event E (b1, b2).

Downloaded from iwaponline.com/hr/article-pdf/57/3/383/1608758/nh2026046.pdf
by Delft University of Technology user

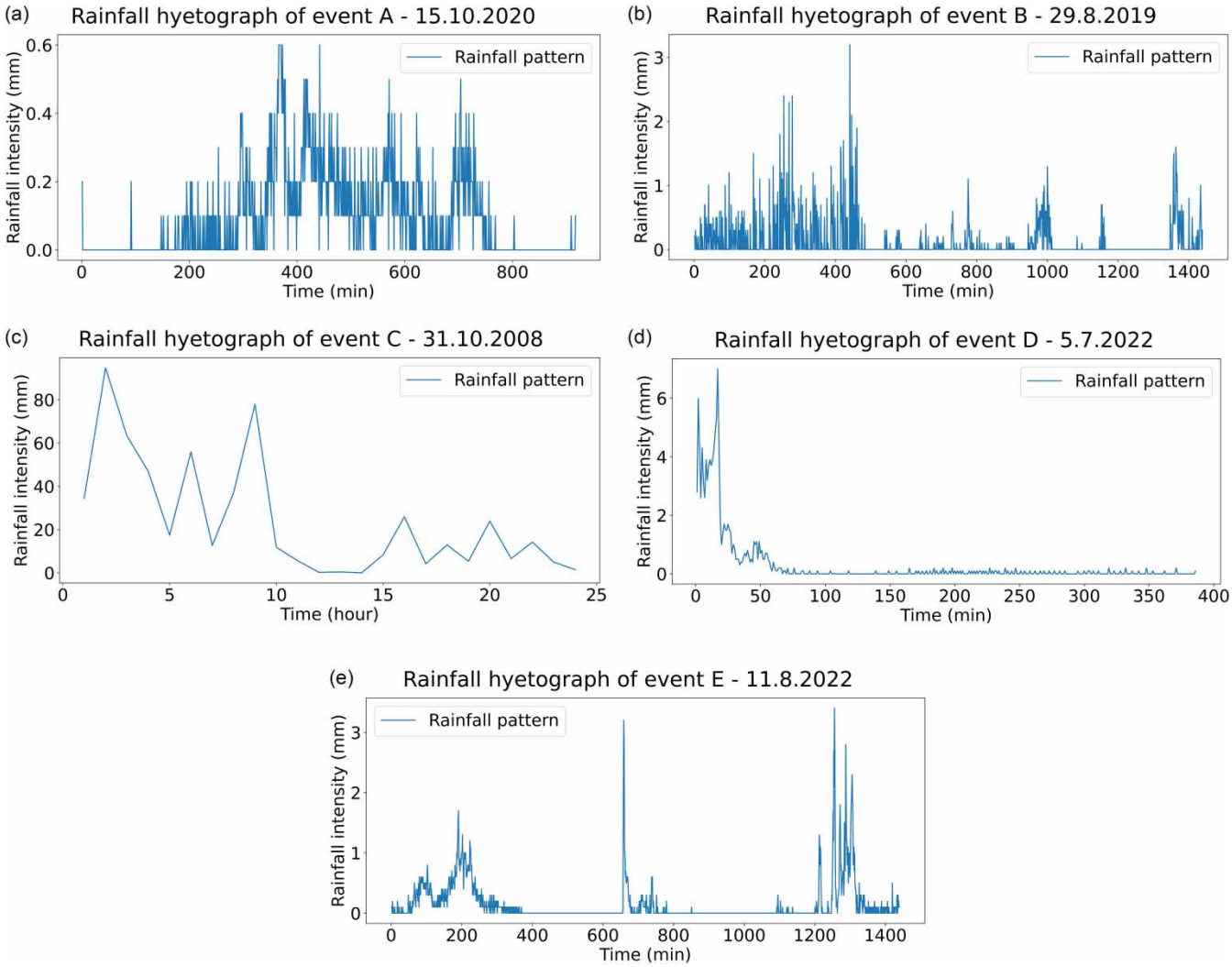


Figure 6 | Actual rainfall distributions in Event A (15.10.2020) (a), Event B (29.8.2019) (b), Event C (31.10.2008) (c), Event D (05.07.2022) (d), and Event E (11.8.2022) (e).

Table 2 | Daily rainfall amounts are equivalent to the chosen return periods

Returned period (year)	1.25	2.0	2.5	5	10	20	50
Daily rainfall amount (mm)	86.91	117.69	133.88	188.32	246.91	308.69	394.52

Spatiotemporal flood analysis using the PNFA

Result processing for a single scenario

A flood assessment period was set in each simulation. The beginning of this period was the moment when the rainfall started. The assessment period concluded either at the time of the last recorded rainfall or when the final flood of the entire region subsided. Flood results from the simulation were extracted into a timeline table, recording data every minute for every key manhole in the system.

The flood situation of Event A was examined thoroughly represented by three nodes N31-17-1, N10-17-1, and N11-46 as a detailed illustration. The node locations are shown in Figure 1(c). In this flood event, some nodes got flooded in the early stage of the rain, such as Node N31-17-1 (Figure 7(b)). Node N31-17-1 experienced the lag time/lapse time between the initial rainfall and initial flood, so-called lag interval (LI) at 191 min. As shown in Figure 7(b), this node also encountered a longer

Downloaded from iwaponline.com/hr/article-pdf/57/3/383/1608758/nh2026046.pdf
by Delft University of Technology user

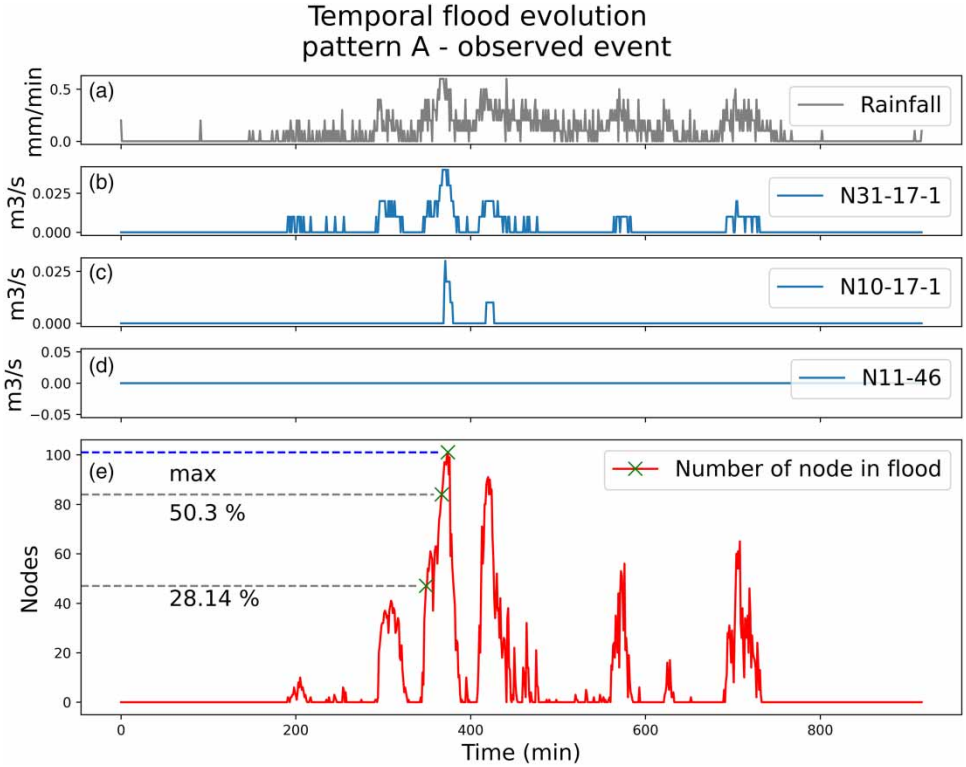


Figure 7 | Flood simulation result extractions from Event A: Rainfall distribution (a); flooding dynamics in node N11-1 (b), N10-17-1 (c), and N11-46 (d); and the number of nodes in flood (e).

flood duration during the assessment period. The surface area on top of this node was also the most vulnerable area with flooding in this area. Simultaneously, some other nodes, like N10-17-1, experienced the flood later and also had a shorter duration of flood (Figure 7(c)). The LI of node N10-17-1 was 370 min. The surface area on top of this node was less vulnerable to flood than node N31-17-1. Meanwhile, several nodes, for example, N11-46, had no flood during the assessment period. This node did not have the LI (Figure 7(d)).

To gain a broader perspective on the flood evolution during the flooding time, the number of nodes in the flood (NNF) was recorded every time step. Figure 7(e) shows the dynamics of NNF during the flooding time. The flood evolution intervals (FEIs) that flood areas reached a certain threshold based on the percentage of nodes in flood (PNF) were defined. As above-mentioned, those thresholds include Q1 25% (~42/167 nodes in the flood), Q2 50% (84/167 nodes in the flood), Q3 75% (126/167 nodes in the flood), Q4 over 75% (over 126/167 nodes in the flood), and Q0 – non-flood quartile (non-flood nodes). In the case of Event A, the maximum NNF were 101 nodes ~ 60.5% PNFs, which was smaller than 75% (Q4). Therefore, in this case, only Q1, Q2, Q3, and Q0 thresholds were considered. No node belonged to the Q4 threshold (above 75% node in the flood). The LI in the whole area is 191 min (Figure 7(e)).

As the flood quartile definition, $FEI_{25\%}$ was the duration when the flood area reached 25% PNF ~ NNF = 42 nodes in the flood. In fact, depending on the rainfall intensity and flood situation, the NNF was not always accurate at 42 nodes. Consequently, to capture the real situation, the very first moment when the PNF was over 25% would be selected to be the first threshold ($FEI_{25\%}$). PNF was also recalculated to fit with the updated selection. So, in the case of the Event A, the selected PNF and FEI are shown in Table 3. A similar process was applied for another 23 scenarios.

Temporal classification for multiple scenarios

To analyse the temporal flood evolution, a temporal flood expansion diagram was built. Each line in the graph reflects the process that the flood rose from zero to the maximum number of nodes in the flood through the timeline. There were three important temporal flood factors needed to consider: PNF, FEI, and LI. Those factors were defined in the previous process.

Downloaded from iwaponline.com/hr/article-pdf/57/3/383/1608758/nh2026046.pdf
by Delft University of Technology user

Table 3 | NNF, PNF, and FEI of flood simulation in Event A

NNF (nodes)	PNF (%)	FEI (min)
47	28.14	349
84	50	367
101	60.5 (max value)	374

Figure 8(a) depicts the flood evolution of three actual rainfall events: A, B, and C. Event A was the least severe in terms of temporal scale, with the lowest maximum PNF (64%), the longest maximum FEI (376 min), and the longest LI (107 min). Event C was the most severe, with the highest maximum PNF (89%), the shortest maximum FEI (95 min), and the shortest LI (2 min). Event B was a moderate event, with an average PNF (72%), FEI (282 min), and LI (5 min). These flood reactions reflect the intensity and amount of rainfall for each event. Since the three rainfall events (A, B, and C) had different return periods (1.25-, 5-, and 300-year, respectively), it was difficult to pinpoint the differences between the three rainfall patterns.

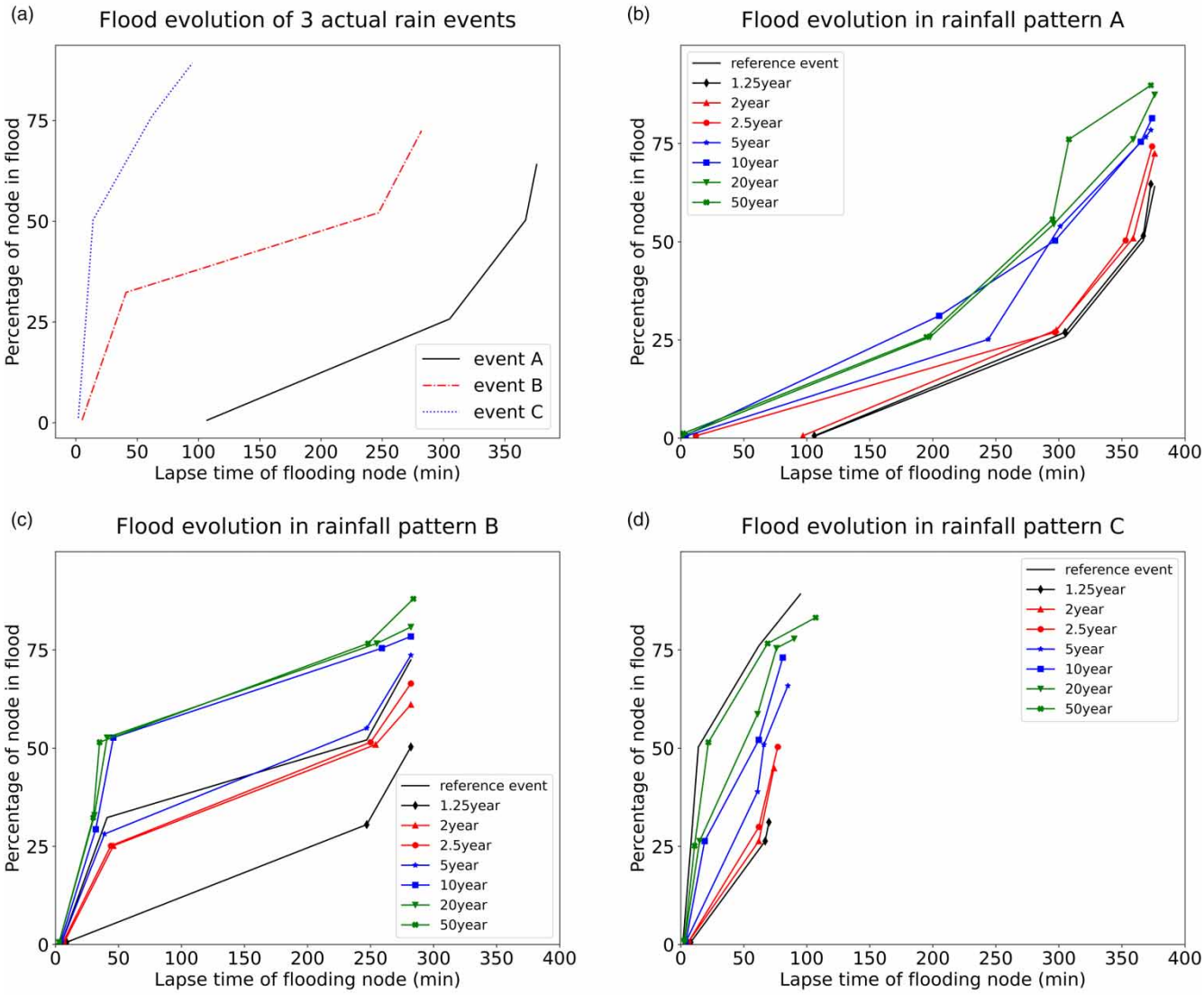


Figure 8 | Temporal flood expansion: comparison of three actual Events A, B, and C (a), with each flood pattern representing different scenarios. Event A (b), Event B (c), and Event C (d).

Downloaded from iwaponline.com/hr/article-pdf/57/3/383/1608758/nh2026046.pdf
by Delft University of Technology user

Figure 8(b)–8(d) shows three comparisons of different rainfall patterns across different scenarios. From these diagrams, it is evident that more intense rainfall results in a higher PNF. However, rainfall intensity seemed to have a lesser effect on the FEI in pattern C (70–149 min), but not in patterns A (373–376 min) and B (282–284 min).

The results show that pattern A, with low return periods (1.25- and 2-year), exhibits a long LI (~100 min), which corresponds to a decrease in rainfall intensity. This extended LI is due to the intermittent rainfall at the start of the assessment period. However, when the rainfall intensity increased, the flooding caused by pattern A occurred almost immediately after the rain began. The limited capacity of the drainage system is believed to be the primary cause of this phenomenon.

To numerically quantify the flood extent spreading speed, FER was calculated, as shown in Figure 9. Pattern A caused the largest flood areas; however, FERs of pattern A were lower than the others. Time for flood preparation/evacuation in pattern A was longer than the other patterns (i.e. patterns B and C).

Spatiotemporal clustering (individual scenario visualization)

Flood quartiles combined with location showed the spatiotemporal distribution of the flood. In Figure 10(a), flooding node locations during event A are shown for different time scales. During these events, the initial areas experiencing flood were divided into three centres, concentrated mostly on the main road AH13 and adjacent regions. Subsequently, the flood gradually extended to the surrounding section of the road and then spread towards the northern part of the area. Notably, the regions near the northern and southern outfalls remained unaffected by floods across the various scenarios. Based on the spatiotemporal flood node locations, a spatiotemporal flood hazard map was generated using the inverse distance weight (IDW) interpolation method (Figure 10(b)). This flood hazard map provides an initial overview of how the flood evolved spatially and temporally during the actual rainfall event A. Flood regions were categorized following temporal flood quartiles (i.e. Q1, Q2, Q3, Q4, and Q0). This spatiotemporal flood distribution gives a different view on flood evolution and flood prevention priority. This complemented the spatial flood distribution, which was built up based on the total flood discharge in each node (Figure 10(c)). Compared with the spatial distribution, the vulnerable areas were enlarged around the main street AH13. Flood areas were concentrated in three areas across the study area. Continuously, the other 23 single flood hazard maps were generated for the other 23 rainfall scenarios, creating a dataset of flood hazard maps (Figure 11(a) and 11(b)).

Figure 11(a) illustrates the temporal evolution of the flood-affected area under the temporal scale. The results indicate that rainfall intensity significantly influences the rate of flooding. Specifically, pattern A resulted in the slowest flood progression, with flooding occurring between 195 and 376 min. In contrast, pattern C induced a flash flood within a much shorter timeframe, ranging from 8 to 107 min. Pattern B produced an intermediate flooding response, with flood onset occurring between 30 and 284 min. Furthermore, when comparing the three rainfall patterns under the same return-period scenario, it is evident that mild rainfall (pattern A) led to a slower flood spread over a larger area than torrential rainfall (pattern C). These findings highlight that the temporal distribution of rainfall, or the shape of the rainfall hyetograph, plays a crucial role in determining flood timing on the ground.

However, although the induced rainfall varies in pattern and intensity, the flood evolutions exhibit a similar pattern across all 24 scenarios under the quartile scale (Figure 11(b)). Regions which are near the outfalls have never experienced flooding. There are some flooding nodes which swing between two quartile ranks (e.g. from Q2 to Q3 and vice versa). Those flexible-in-rank nodes created the slight differences between various scenarios. Nevertheless, in brief, the flood in the research area evolved in a certain pattern. This means that the spatiotemporal flood analysis is stable and reliable to use in flood risk assessment.

For more details, although the main spatiotemporal flood pattern remained unchanged, there were still slight differences in flood distributions caused by different rainfalls. Rainfall pattern A had a larger affected area than the other patterns within the same return-period scenarios, whereas rainfall pattern C, with the same return-period scenario, caused flooding in the smallest area. The flood simulation results from rainfall pattern C were contrary to expectations based on the historical rainstorm data. For example, within the 1.25-year return period, pattern C caused flooding in 52 nodes, approximately 31% of the observed nodes in the research area. Meanwhile, pattern B and pattern A caused flooding in 84 nodes (~50.3%) and 108 nodes (~64.7%), respectively. More details are shown in Figure 9(b). This trend was consistent across other scenarios (Figure 11(b)). Rainfall intensity is believed to be the primary factor driving this phenomenon. In fact, rainfall pattern A had a milder intensity than rainfall pattern C. In conclusion, the same amount of rainfall over a shorter period resulted in a more concentrated flood area than when it occurred over a longer period. Consequently, the spatiotemporal flood hazard maps also reflect these slight differences.

Downloaded from iwaponline.com/hr/article-pdf/57/3/383/1608758/nh2026046.pdf
by Delft University of Technology user

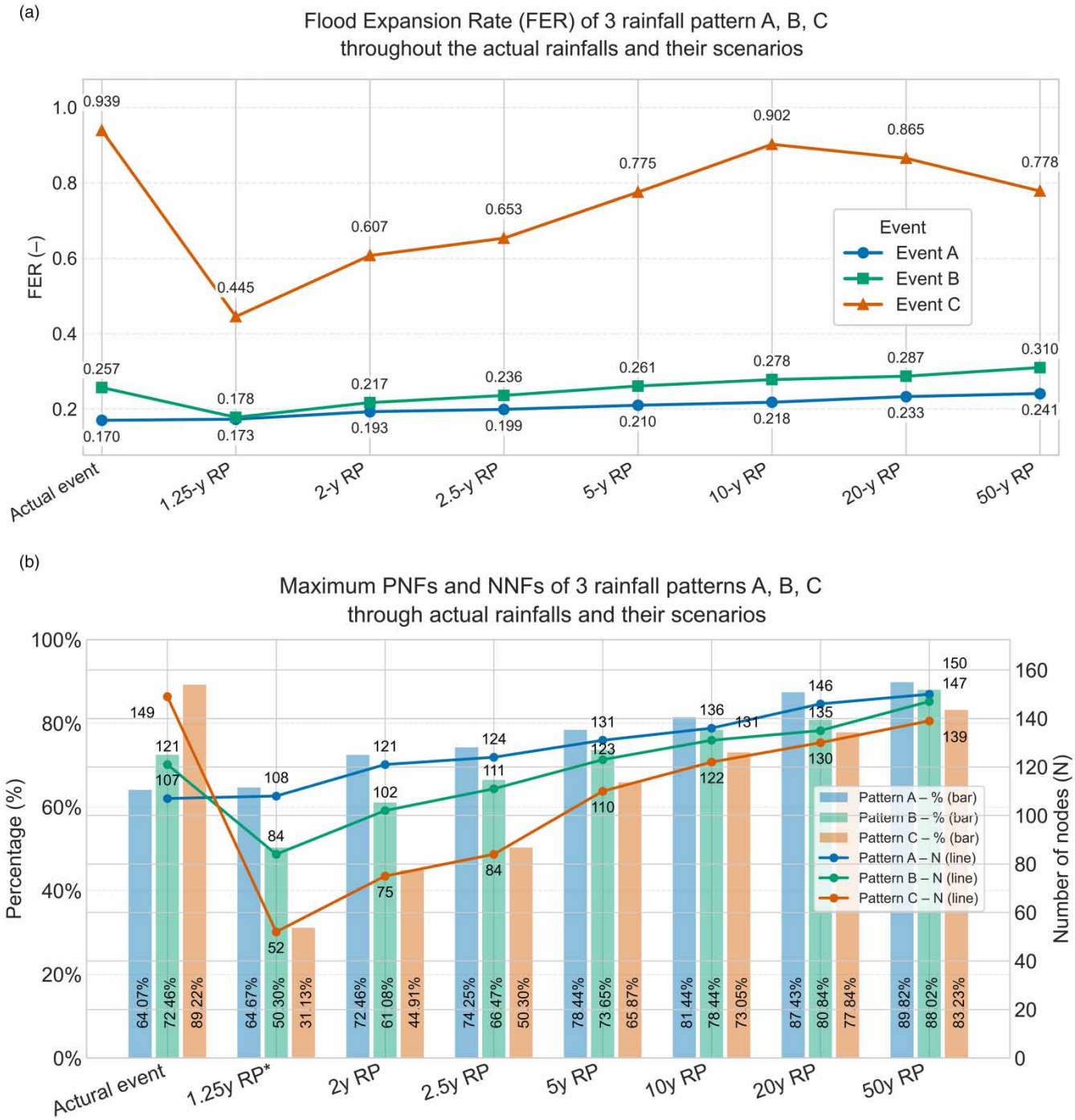


Figure 9 | Comparison indicators among the three rainfall patterns, A, B, and C and their scenarios: (a) FER and (b) PNFs and NNFs (-y RP: year Return Period).

Aggregated spatiotemporal flood distribution

In the previous step, flood distributions were examined by 24 different scenarios. Similar spatiotemporal flood patterns were found across various scenarios. The spatiotemporal flood hazard evolution remained stable throughout the different scenarios. In addition, the flood-affected areas among the three rain patterns differed slightly, despite being simulated under the same return period. Therefore, in order to get a holistic view of the flood evolution, flood distributions during 24 scenarios were overlaid and aggregated to create a spatiotemporal flood hazard map.

Downloaded from iwaponline.com/hr/article-pdf/57/3/383/1608758/nh2026046.pdf
by Delft University of Technology user

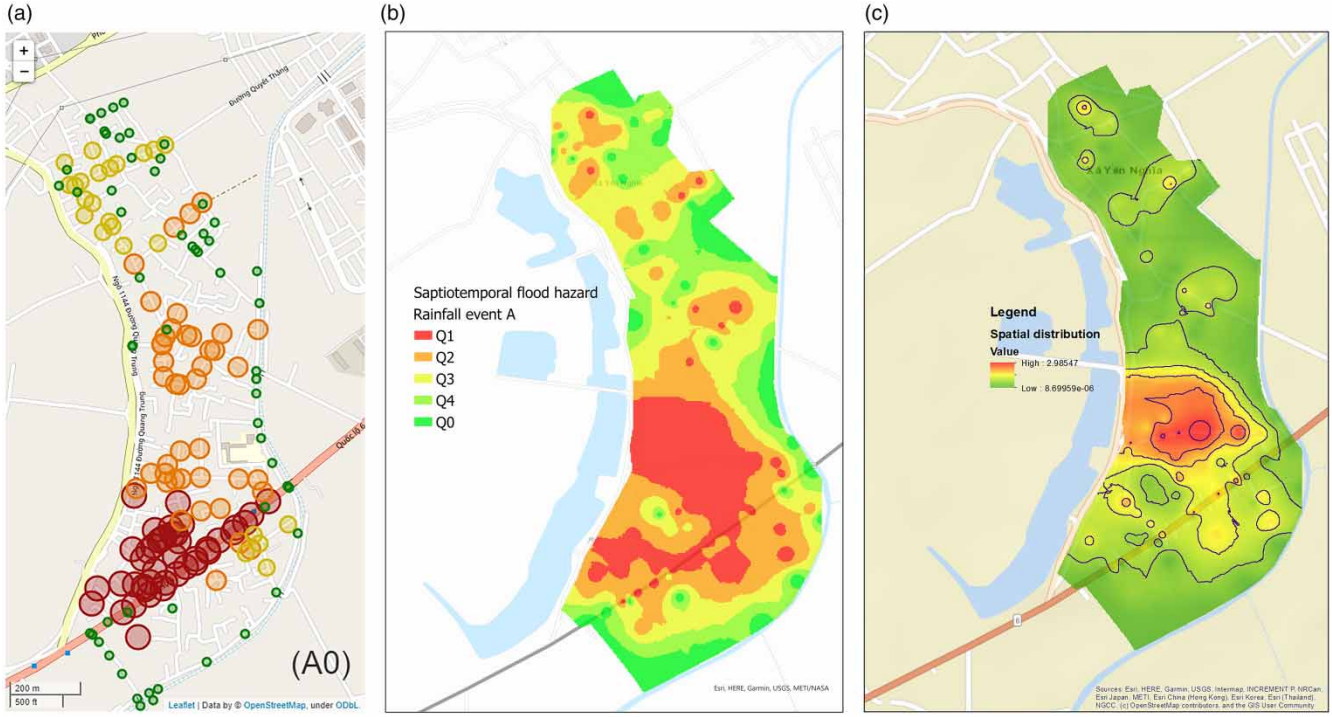


Figure 10 | Historical Event A: (a) spatiotemporal flood node locations, (b) spatiotemporal flood distribution, and (c) spatial flood distribution.

Figure 12(a) shows the most critical spatiotemporal hazard and its associated probabilities. Flooding at each node can vary across different categories of spatiotemporal distribution. The most critical situation corresponds to the fastest flood category, which is most likely to occur across all 24 scenarios. The probability of this critical situation is also depicted on the map.

Similarly, the high-potential spatiotemporal flood hazard is presented in Figure 12(b). Its probability is also shown in this map. These two maps highlight the vulnerable locations in the research area where experienced flood spatially and temporally, as well as the potential flood evolutions. These maps can be valuable for stakeholders, such as drainage system companies, in maintaining the drainage infrastructure and optimizing the allocation of human resources during flooding events. They can help address the issue of human resource shortages during such times. On the other hand, these two maps can serve as an initial foundation for implementing nature-based solutions, as they identify temporally sensitive areas.

DISCUSSION

Temporal analysis

Temporal flood analysis is the initial step to characterize the flood hazard in the area. The FER serves as an initial and straightforward coefficient for gauging flood propagation speed or agility, offering a numerical basis for comparing flood dynamics across varying timescales. During one rainfall event, the flood risk to pedestrians is different over time during the rainfall event (Corzo Perez *et al.* 2024). The FER, which represents flood severity, was used to quantify the magnitude of the flood over time during the rainfall. Additionally, FER serves as a global indicator that allows for the comparison of flood speeds across various events, regardless of rainfall duration. The higher the FER, the faster and more dangerous the flood, irrespective of the rainfall interval. FER reflects the speed at which the flood spreads spatially, an important factor to consider in flood assessments, particularly in flash flood evaluations.

Generally, in flood hazard assessments, the flood spreading speed is not included. Flood interventions, especially Nature-based Solutions (NbS), focus on slowing down the surface runoff (Esraz-Ul-Zannat *et al.* 2024). Responding to flash floods requires not only proper preparedness before the event but also a rapid response during the flood incidents (Archer & Fowler 2018). Time is a critical factor in managing flash floods, especially when human resources are limited. Therefore, it is essential to have a measurable tool to assess flood agility and the effectiveness of flood prevention measures. In this

Downloaded from iwaponline.com/hr/article-pdf/57/3/383/1608758/nh2026046.pdf
by Delft University of Technology user

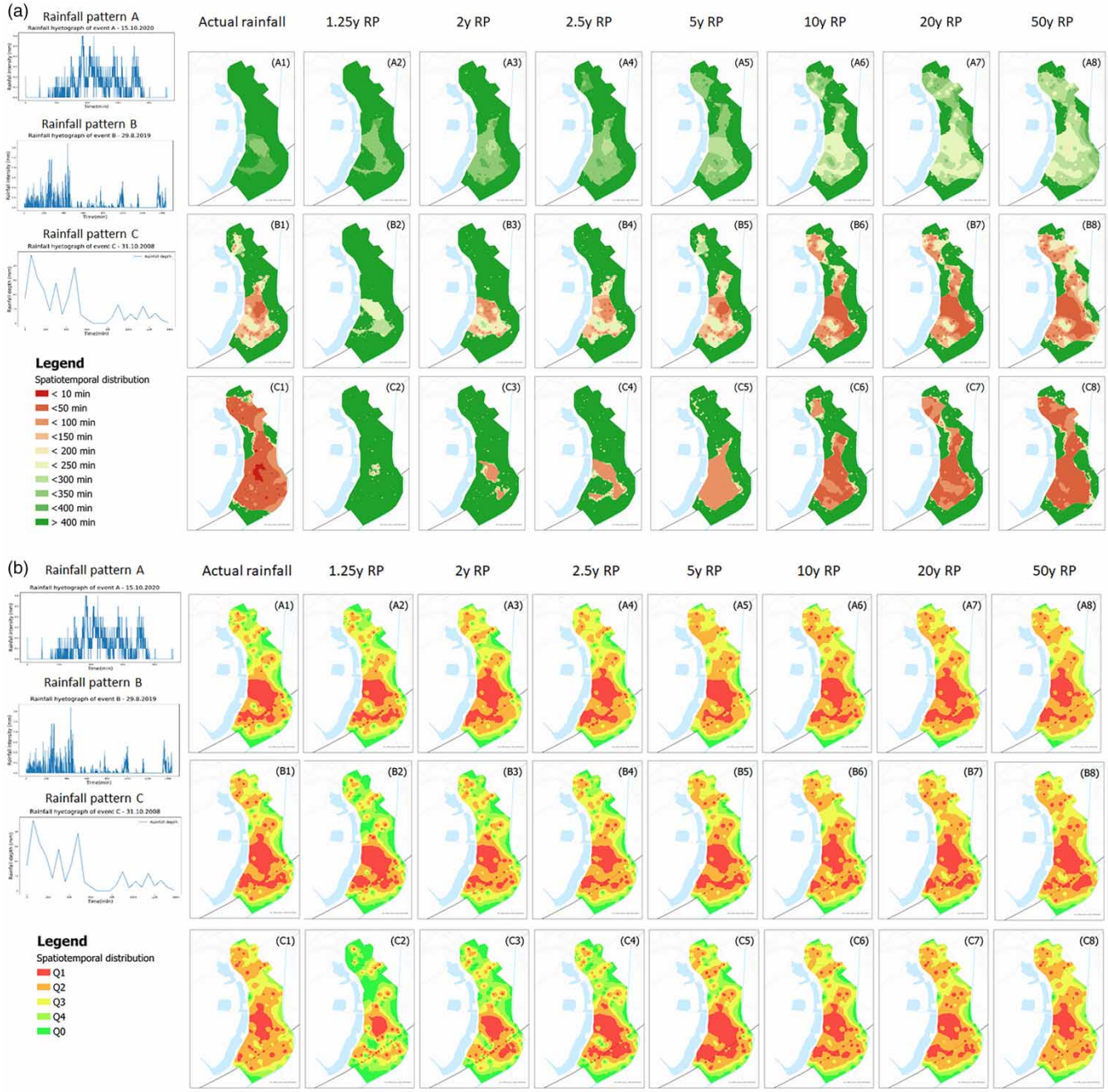


Figure 11 | Spatiotemporal flood hazards in 24 scenarios of three rainfall patterns (i.e. A, B, and C) with eight scenarios (i.e., 1.25-, 2-, 2.5-, 5-, 10-, 20-, 50-year return period, and actual rainfall distribution) with timescale (a) and with quantile scales (b) (y RP: year Return Period).

context, FER fulfils this requirement. In addition, while FER assesses the speed of flood spreading, the LI plays a crucial role in mitigating the flood's impact. As shown in the experiments, the longer the lag time (i.e., LI), the lower the FER. In other words, a longer lag time helps reduce the speed at which the flood expands in urban areas. By extending the LI, residents and organizations in flood-prone regions would gain valuable time for preparation and evacuation. Therefore, this temporal buffer is key to enhancing community resilience against flooding events. Lengthening the LI could be an important strategy for mitigating flood impacts. It is recommended to assess the influence of LI on flood reactions in urban areas to design more effective flood interventions and reduce overall flood impact.

Downloaded from iwaponline.com/hr/article-pdf/57/3/383/1608758/nh2026046.pdf
by Delft University of Technology user

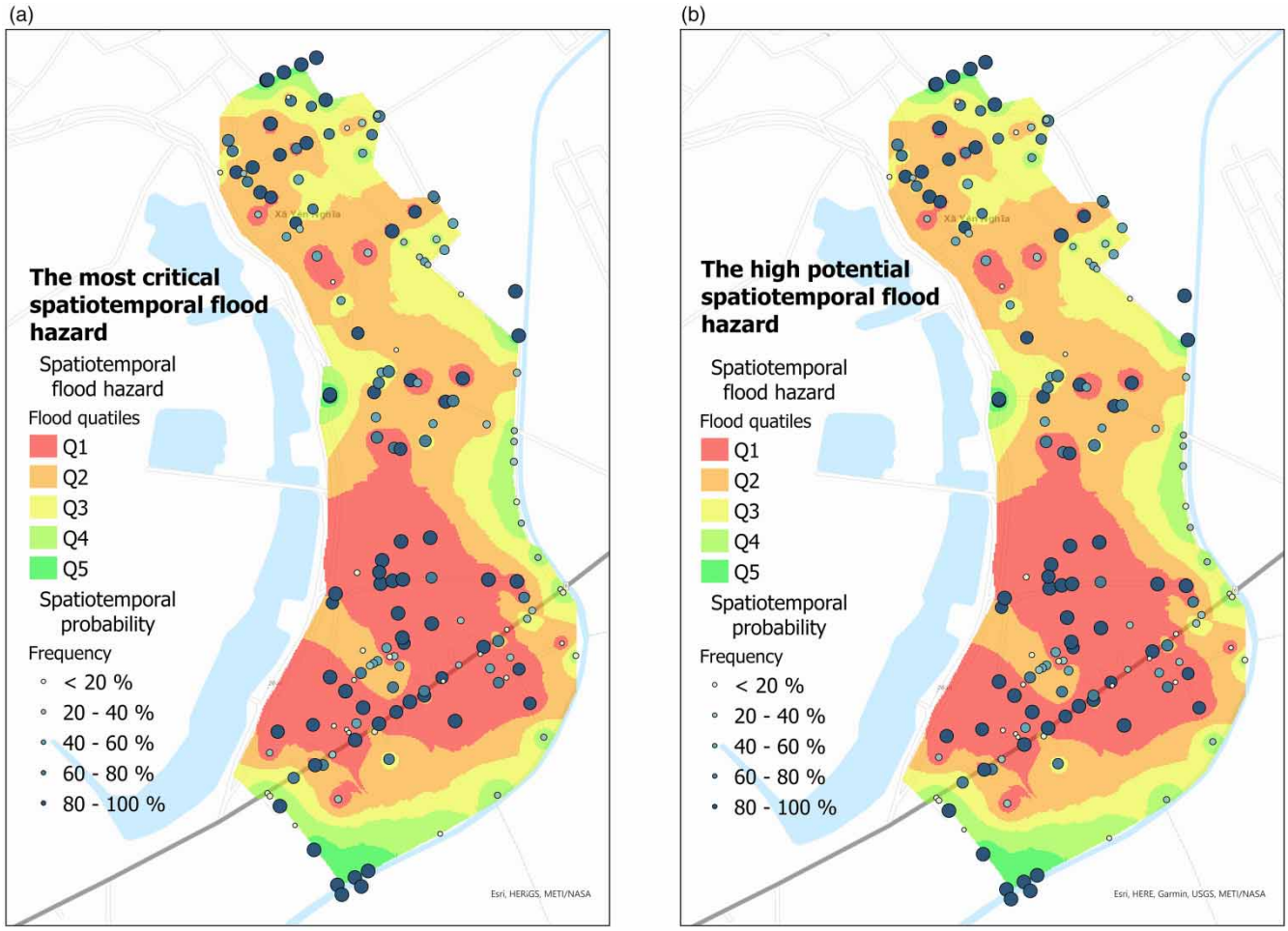


Figure 12 | Aggregated spatiotemporal flood hazard: (a) the most critical spatiotemporal flood hazard and (b) the most probable spatiotemporal flood hazard.

Spatiotemporal analysis

Besides the temporal analysis, the spatiotemporal analysis provided a new perspective on the spatial distribution of floods, integrating temporal dynamics into the assessment framework. By accounting for flood sequences, the analytical approach followed here enabled the identification of areas prone to flooding over time, thus reshaping the priorities in flood management, particularly in the context of the rapid onset of extreme events. The selection and design of flood interventions needs to take into account the temporary exposure of both the citizens (e.g. traffic travellers) and the permanent residents in flood-prone areas. Spatiotemporal flood evolution gives a holistic overview of the flood progress in both space and time during the flooding time. This insight is vital to allocating human resources efficiently. Particularly, this information is very important both for stakeholders and citizens who live in a flood-prone area for the development of an evacuation plan (Lee *et al.* 2020). It will enable stakeholders, such as a drainage system company, to allocate human resources during the rainfall event in order to improve the effectiveness of maintenance plans.

Spatiotemporal flood distribution pattern analysis

Spatiotemporal flood distribution pattern analysis, compared with the use of solely static topographic maps, reveals that initial flood-affected locations may not necessarily coincide with areas of lowest elevation. Drainage efficiency decreases the flood risk of an area. This observation underscores the influence of the drainage system capacity on the flooding dynamics. It also reveals that high-intensity rainfall over a short period, or torrential rain, caused flooding in more concentrated areas. This highlights the sensitive regions vulnerable to flash floods in urban areas.

Downloaded from iwaponline.com/hr/article-pdf/57/3/383/1608758/nh2026046.pdf
by Delft University of Technology user

In addition, flood mitigation remedies must consider the cost-benefit balance. The size and location of interventions (i.e. swales, detention, and retention) involve a spatial trade-off in urban planning design (Bush & Doyon 2019). By incorporating a timescale, spatiotemporal flood distribution increases the efficiency of the potential flood interventions.

This study showed that flooding caused by the historical rainstorm (pattern C) did not result in a high flood risk in low-intensity scenarios (i.e., 1.25-, 2-, 2.5-, 5-, and 10-year return periods). The rainfall distribution interval (1 h) appears to be the main factor behind this phenomenon. While pattern C has a 1-h interval between rainfall events, patterns A and B have a 1-min interval.

Limitations

Nevertheless, this study has still revealed some limitations. Firstly, this research relied on daily rainfall data for generating extreme rainfall events in the Monte Carlo simulations. While this ensures statistical reliability over a long period, it may smooth out short-duration, high-intensity peaks typically observed during monsoon events. As a result, the fixed hyetograph shape, while useful for general event simulation, might underestimate sub-daily peak intensities. This should be considered when interpreting the results, particularly for applications like urban flood modelling, where short-duration rainfall extremes can have significant impacts. Secondly, spatiotemporal flood distribution used the IDW interpolation method, which is only based on the distance relation between the 1D spatiotemporal flood results. This method has not yet taken into account the influence of DEM on the flood propagation. It is a trade-off between the speed and the accuracy of the modelling process. It is recommended to further research on a 2D model, which includes the DEM influence on the flood simulation. Furthermore, it is crucial to acknowledge that this study does not cover the entire spectrum of flood risk management. Factors, such as socio-economic vulnerability and infrastructural resilience, which are equally vital components, should also be included to ensure a comprehensive flood risk assessment.

Future works

Although this work introduces a new approach for analysing floods that reshapes flood assessments, there is still room for further exploration. Firstly, the two new indicators (i.e. FER and LI) require further study to better understand their influence on urban flood response. Engaging these two indicators in the design of NbS could boost the efficiency of these measurements. Secondly, applying the spatiotemporal analysis to a 2D model could enhance the quality of flood prediction. However, there may be a trade-off between modelling speed and accuracy when comparing the spatiotemporal 1D model and the spatiotemporal 2D model that needs to be considered. Monitoring urban flood data (e.g. floodwater quantity and quality) remain challenging due to limited human resources and the unpredictable distribution of rainfall. Therefore, the application of new technologies, such as machine learning and AI, could help reduce both the time and cost associated with flood research. Engaging citizens in data collection through crowdsourcing offers a potential solution to human resource shortages. This win-win approach benefits both citizens and researchers, providing a promising opportunity for effective data monitoring.

CONCLUSION

This study advances urban flood hazard assessment by introducing a spatiotemporal analytical framework comprising three core components: (i) temporal flood evolution, (ii) spatiotemporal hazard mapping, and (iii) the FER as a quantitative indicator. FER values, ranging from 0.17 (slow) to 0.902 (rapid), effectively characterize the rate of flood propagation and associated flood severity. The analysis demonstrates that flood expansion patterns remain consistent across varying rainfall intensities, hyetographs, and return periods, underscoring the robustness of the proposed methodology. Critical flood-prone zones, particularly along the AH13 highway, were identified as requiring prioritized intervention, whereas the northern drainage network exhibited high efficiency attributable to its structural design.

By integrating temporal dynamics into conventional spatial assessments, this approach enhances the precision and timeliness of flood hazard evaluation. The resulting temporal evolution diagrams and spatiotemporal hazard maps provide actionable insights for stakeholders, facilitating proactive and adaptive flood management strategies. FERs – as a numeric quantified indicator, can be used as a global comparable measure for FER between different rainfall events. Furthermore, the findings reveal that flood behaviour is influenced by factors beyond topographic elevation, highlighting the complexity of urban hydrological processes. Although the direct impacts of individual flood events were beyond the scope of this study, the results delineate recurrent flood hotspots and infrastructure vulnerabilities, offering a basis for targeted drainage improvements and mitigation planning.

Downloaded from iwaponline.com/hr/article-pdf/57/3/383/1608758/nh2026046.pdf
by Delft University of Technology user

Overall, this research contributes to a deeper understanding of urban flood dynamics, validates the utility of spatiotemporal analysis in risk assessment, and establishes a foundation for future investigations aimed at quantifying flood impacts and refining urban flood management practices.

ACKNOWLEDGEMENTS

The authors would like to thank the Ministry of Infrastructure and Water Management – The Netherlands, IHE Delft Institute for Water Education – The Netherlands, The Viet Nam Government, Hanoi Drainage and Sewage System Company (HSDC) – Viet Nam, Hanoi Architectural University – Viet Nam, Ha Dong District People committee – Viet Nam, Yen Nghia Commune People Committee – Viet Nam and Yen Nghia citizens for supporting this research. This statement, contained within the manuscript/research article, is not the opinion of the funding agency, the Viet Nam Government or the Dutch Government, but reflects the author's opinions. The authors extend their gratitude to the reviewers for their insightful comments and valuable contributions to improving this manuscript.

FUNDING

This study is supported by Project 911 of the Ministry of Education and Training – Viet Nam and the Ministry of Infrastructure and Water Management – The Netherlands.

AUTHOR CONTRIBUTIONS

Conceptualization: H.D.M. and G.A.C.P.; methodology: H.D.M. and G.A.C.P.; software: H.D.M. and W.B.; formal analysis: H.D.M. and G.A.C.P.; investigation: H.D.M., G.A.C.P., and W.B.; data curation: H.D.M.; writing – original draft preparation: H.D.M; writing – review and editing: H.D.M., G.A.C.P., W.B., and C.Z.; funding acquisition: H.D.M. and G.A.C.P.

DATA AVAILABILITY STATEMENT

Data cannot be made publicly available; readers should contact the corresponding author for details.

CONFLICT OF INTEREST

The authors declare there is no conflict.

REFERENCES

Abass, K., Dumedah, G., Frempong, F., Muntaka, A. S., Appiah, D. O., Garsonu, E. K. & Gyasi, R. M. (2022) Rising incidence and risks of floods in urban Ghana: is climate change to blame? *Cities*, **121**, 103495. https://doi.org/10.1016/j.cities.2021.103495.

Abedin, J., Zou, L., Yang, M., Rohli, R., Mandal, D., Qiang, Y., Akter, H., Zhou, B., Lin, B. & Cai, H. (2024) Deciphering spatial-temporal dynamics of flood exposure in the United States, *Sustainable Cities and Society*, **108**, 105444. https://doi.org/10.1016/j.scs.2024.105444.

Acosta-Coll, M., Ballester-Merelo, F., Martinez-Peiró, M. & De la Hoz-Franco, E. (2018) Real-time early warning system design for pluvial flash floods – a review, *Sensors (Switzerland)*, **18** (7), 2255. https://doi.org/10.3390/s18072255.

Afsari, R., Nadizadeh Shorabeh, S., Kouhnavard, M., Homaee, M. & Arsanjani, J. J. (2022) A spatial decision support approach for flood vulnerability analysis in urban areas: a case study of Tehran, *ISPRS International Journal of Geo-Information*, **11** (7), 380. https://doi.org/10.3390/ijgi11070380.

Al-Rawas, G., Nikoo, M. R. & Al-Wardy, M. (2024) A review on the prevention and control of flash flood hazards on a global scale: early warning systems, vulnerability assessment, environmental, and public health burden, *International Journal of Disaster Risk Reduction*, **115**, 105024. https://doi.org/10.1016/j.ijdrr.2024.105024.

Alves, P. B. R., Amanguah, E., McNally, D., Espinoza, M., Ghaedi, H., Reilly, A. C. & Hendricks, M. D. (2024) Navigating the definition of urban flooding: a conceptual and systematic review of the literature, *Water Science and Technology*, **90** (10), 2796–2812. https://doi.org/10.2166/wst.2024.351.

Amornsiripanitch, N., Biswas, S., Orellana-Li, J. & Zink, D. (2025) Measuring flood underinsurance in the USA, *Nature Climate Change*, **15** (9), 971–977. https://doi.org/10.1038/s41558-025-02396-w.

Angelakis, A. N., Capodaglio, A. G., Valipour, M., Krasilnikoff, J., Ahmed, A. T., Mandi, L., Tzanakakis, V. A., Baba, A., Kumar, R., Zheng, X., Min, Z., Han, M., Turay, B., Bilgiç, E. & Dercas, N. (2023) Evolution of floods: from ancient times to the present times (ca 7600 BC to the present) and the future, *Land*, **12** (6), 1211. https://doi.org/10.3390/land12061211.

Archer, D. R. & Fowler, H. J. (2018) Characterising flash flood response to intense rainfall and impacts using historical information and gauged data in Britain, *Journal of Flood Risk Management*, **11**, S121–S133. https://doi.org/10.1111/jfr3.12187.

Downloaded from iwaponline.com/hr/article-pdf/57/3/383/1608758/nh2026046.pdf
by Delft University of Technology user

Arrighi, C., Oumeraci, H. & Castelli, F. (2017) Hydrodynamics of pedestrians' instability in floodwaters, *Hydrology and Earth System Sciences*, **21** (1), 515–531. https://doi.org/10.5194/hess-21-515-2017.

Beg, M., Rubinato, M., Carvalho, R. & Shucksmith, J. (2020) CFD modelling of the transport of soluble pollutants from sewer networks to surface flows during urban flood events, *Water (Switzerland)*, **12** (9), 2514. https://doi.org/10.3390/w12092514.

Bentivoglio, R., Isufi, E., Jonkman, S. N. & Taormina, R. (2023) Rapid spatio-temporal flood modelling via hydraulics-based graph neural networks, *Hydrology and Earth System Sciences*, **27** (23), 4227–4246. https://doi.org/10.5194/hess-27-4227-2023.

Berkhahn, S. & Neuweiler, I. (2024) Data driven real-time prediction of urban floods with spatial and temporal distribution, *Journal of Hydrology X*, **22**, 100167. https://doi.org/10.1016/j.hydroa.2023.100167.

Bernardini, G., Ferreira, T. M., Baquedano Julià, P., Ramírez Eudave, R. & Quagliarini, E. (2024) Assessing the spatiotemporal impact of users' exposure and vulnerability to flood risk in urban built environments, *Sustainable Cities and Society*, **100**, 105043. https://doi.org/10.1016/j.scs.2023.105043.

Bush, J. & Doyon, A. (2019) Building urban resilience with nature-based solutions: how can urban planning contribute? *Cities*, **95**, 102483. https://doi.org/10.1016/j.cities.2019.102483.

Cao, X., Wang, B., Yao, Y., Zhang, L., Xing, Y., Mao, J., Zhang, R., Fu, G., Borthwick, A. G. L. & Qin, H. (2025) U-RNN high-resolution spatiotemporal nowcasting of urban flooding, *Journal of Hydrology*, **659**, 133117. https://doi.org/10.1016/j.jhydrol.2025.133117.

Cea, L., Sañudo, E., Montalvo, C., Farfán, J., Puertas, J. & Tamagnone, P. (2025) Recent advances and future challenges in urban pluvial flood modelling, *Urban Water Journal*, **22** (2), 149–173. https://doi.org/10.1080/1573062X.2024.2446528.

Chen, X.-Z., Lu, Q.-C., Peng, Z.-R. & Ash, J. E. (2015) Analysis of transportation network vulnerability under flooding disasters, *Transportation Research Record*, **2532** (1), 37–44. https://doi.org/10.3141/2532-05.

Corzo Perez, G. A., Sanchez Tapiero, D. I., Contreras Martínez, M. A. & Zevenbergen, C. (2024) Development of a hazard risk map for assessing pedestrian risk in urban flash floods: a case study in Cúcuta, Colombia, *River*, **3** (1), 8–23. https://doi.org/10.1002/rvr2.78.

CRED (2025) *2024 Disasters in Numbers*. Brussels: Centre for Research on the Epidemiology of Disasters.

Darnkachatarn, S. & Kajitani, Y. (2024) Long-term flood exposure assessment using satellite-based land use change detection and inundation simulation: a 30-year case study of the Bangkok Metropolitan Region, *Journal of Flood Risk Management*, **17** (3), 1–16. https://doi.org/10.1111/jfr3.12997.

Do Minh, H., Perez, G. C., Barreto, W. & Zevenbergen, C. (2023) A spatiotemporal hydrological response of extreme urban floods in Ha Noi – Vietnam, *Vienna, Austria: eGU General Assembly 2023*, Vienna, Austria, 24–28 April 2023, pp. EGU23–E6891.

Dong, B., Xia, J., Li, Q. & Zhou, M. (2022) Risk assessment for people and vehicles in an extreme urban flood: case study of the '7.20' flood event in Zhengzhou, China, *International Journal of Disaster Risk Reduction*, **80**, 103205. https://doi.org/10.1016/j.ijdrr.2022.103205.

England, J. F., Cohn, T. A., Faber, B. A., Stedinger, J. R., Thomas, W. O., Veilleux, A. G., Kiang, J. E. & Mason, R. R. (2019) *Guidelines for Determining Flood Flow Frequency-Bulletin 17C*. U.S. Geological Survey Techniques and Methods, Book 4, Chap. B5. Reston, VA: US Geological Survey.

Esraz-Ul-Zannat, M., Dedekorkut-Howes, A. & Morgan, E. A. (2024) A review of nature-based infrastructures and their effectiveness for urban flood risk mitigation, *Wiley Interdisciplinary Reviews: Climate Change*, **15**, 1–28. https://doi.org/10.1002/wcc.889.

Fang, B., Bevacqua, E., Rakovec, O. & Zscheischler, J. (2024) An increase in the spatial extent of European floods over the last 70 years, *Hydrology and Earth System Sciences*, **28** (16), 3755–3775. https://doi.org/10.5194/hess-28-3755-2024.

Fernández-Nóvoa, D., González-Cao, J. & García-Feal, O. (2024) Enhancing flood risk management: a comprehensive review on flood early warning systems with emphasis on numerical modeling, *Water (Switzerland)*, **16** (10), 1408. https://doi.org/10.3390/w16101408.

Francipane, A., Pumo, D., Sinagra, M., La Loggia, G. & Noto, L. V. (2021) A paradigm of extreme rainfall pluvial floods in complex urban areas: the flood event of 15 July 2020 in Palermo (Italy), *Natural Hazards and Earth System Sciences*, **21** (8), 2563–2580. https://doi.org/10.5194/nhess-21-2563-2021.

Genovese, E. & Thaler, T. (2020) The benefits of flood mitigation strategies: effectiveness of integrated protection measures, *AIMS Geosciences*, **6** (4), 459–472. https://doi.org/10.3934/geosci.2020025.

Getirana, A., Mandarino, F., Ney de Montezuma, P. & Kirschbaum, D. (2023) An urban drainage scheme for large-scale flood models, *Journal of Hydrology*, **627** (PA), 130410. https://doi.org/10.1016/j.jhydrol.2023.130410.

Hauser, M., Reinstaller, S., Oberascher, M., Muschalla, D. & Kleidorfer, M. (2024) The impact of underground structures on urban flood models, *Water (Switzerland)*, **16** (1), 1–12. https://doi.org/10.3390/w16010170.

Henonin, J., Russo, B., Mark, O. & Gourbesville, P. (2013) Real-time urban flood forecasting and modelling – a state of the art, *Journal of Hydroinformatics*, **15** (3), 717–736. https://doi.org/10.2166/hydro.2013.132.

Ho, T., Phan, V., Le, N. & Nguyen, Q. (2011) Extreme climatic events over Vietnam from observational data and RegCM3 projections, *Climate Research*, **49** (2), 87–100. https://doi.org/10.3354/cr01021.

Huynh, T. T. N., Nguyen, H. Q., Vinh, P. V., Baker, S. & Pathirana, A. (2019) Enteric pathogens in flood-related waters in urban areas of the Vietnamese Mekong Delta: a case study of Ninh Kieu district, Can Tho city, *Urban Water Journal*, **16** (9), 634–641. https://doi.org/10.1080/1573062X.2020.1713381.

Jonkman, S. N., Curran, A. & Bouwer, L. M. (2024) Floods have become less deadly: an analysis of global flood fatalities 1975–2022, *Natural Hazards*, **120** (7), 6327–6342. https://doi.org/10.1007/s11069-024-06444-0.

Kuller, M., Schoenholzer, K. & Lienert, J. (2021) Creating effective flood warnings: a framework from a critical review, *Journal of Hydrology*, **602**, 126708. https://doi.org/10.1016/j.jhydrol.2021.126708.

Downloaded from iwaponline.com/hr/article-pdf/57/3/383/1608758/nh2026046.pdf
by Delft University of Technology user

Lameche, E. K., Boutaghane, H., Saber, M., Abdrabo, K. I., Bermad, A. M., Djeddou, M., Boulmaiz, T., Kantoush, S. A. & Sumi, T. (2023) Urban flood numerical modeling and hydraulic performance of a drainage network: a case study in Algiers, Algeria, *Water Science and Technology*, **88** (7), 1635–1656. https://doi.org/10.2166/wst.2023.277.

Leandro, J., Chen, A. S., Djordjević, S. & Savić, D. A. (2009) Comparison of 1D/1D and 1D/2D coupled (sewer/surface) hydraulic models for urban flood simulation, *Journal of Hydraulic Engineering*, **135** (6), 495–504. https://doi.org/10.1061/(ASCE)HY.1943-7900.0000037.

Leandro, J., Schumann, A. & Pfister, A. (2016) A step towards considering the spatial heterogeneity of urban key features in urban hydrology flood modelling, *Journal of Hydrology*, **535**, 356–365. https://doi.org/10.1016/j.jhydrol.2016.01.060.

Lee, Y. H., Kim, H. I., Han, K. Y. & Hong, W. H. (2020) Flood evacuation routes based on spatiotemporal inundation risk assessment, *Water (Switzerland)*, **12** (8), 2271. https://doi.org/10.3390/w12082271.

Levin, N. & Phinn, S. (2022) Assessing the 2022 flood impacts in Queensland combining daytime and nighttime optical and imaging radar data, *Remote Sensing*, **14** (19), 5009. https://doi.org/10.3390/rs14195009.

Li, Q., Xia, J., Dong, B., Liu, Y. & Wang, X. (2023) Risk assessment of individuals exposed to urban floods, *International Journal of Disaster Risk Reduction*, **88**, 103599. https://doi.org/10.1016/j.ijdrr.2023.103599.

Liang, C., Guan, M., Guo, K., Yu, D. & Yin, J. (2026) Dynamic flood risk modeling in urban metro systems considering station configuration, *Reliability Engineering and System Safety*, **266**, 111760. https://doi.org/10.1016/j.ress.2025.111760.

Liu, T., Shi, P. & Fang, J. (2022) Spatiotemporal variation in global floods with different affected areas and the contribution of influencing factors to flood-induced mortality (1985–2019), *Natural Hazards*, **111** (3), 2601–2625. https://doi.org/10.1007/s11069-021-05150-5.

Lu, X., Chan, F. K. S., Chan, H. K. & Chen, W.-Q. (2023) Investigation of transport logistics disruptions from urban floods: a case study of the Chinese coastal megacity – Guangzhou, China, Lecture Notes in Production Engineering. In: Huang, C.-Y., Dekkers, R., Chiu, S. F., Popescu, D. & Quezada, L. (eds). *Proceedings of the 26th Conference on Production Research*. New York: Springer International Publishing, pp. 637–647. https://doi.org/10.1007/978-3-031-18641-7_59.

Luo, P., Mu, D., Xue, H., Ngo-Duc, T., Dang-Dinh, K., Takara, K., Nover, D. & Schladow, G. (2018) Flood inundation assessment for the Hanoi Central Area, Vietnam under historical and extreme rainfall conditions, *Scientific Reports*, **8** (1), 1–11. https://doi.org/10.1038/s41598-018-30024-5.

Mahiddin, N. A., Umar, R. & Rajan, N. (2023) Rising water, rising voices: empowering communities through the flood emergency response plan, *E3S Web of Conferences*, **437**, 1–9. https://doi.org/10.1051/e3sconf/202343702009.

Miller, J. D. & Hutchins, M. (2017) The impacts of urbanisation and climate change on urban flooding and urban water quality: a review of the evidence concerning the United Kingdom, *Journal of Hydrology: Regional Studies*, **12**, 345–362. https://doi.org/10.1016/j.ejrh.2017.06.006.

Ministry of Construction of Viet Nam (2006) *Water Supply – Distribution System and Facilities Design Standard: TCVN 33:2006 (06/2006/QĐ-BXD)*. Vietnam: Construction Publishing.

Mishra, S. P., Sethi, K. C. & Siddique, M. (2020) Emerging threats during anthropocene as urban flooding of Bhubaneswar city, India, *Water and Energy International*, **63r** (1), 46–58.

Mishra, A., Mukherjee, S., Merz, B., Singh, V. P., Wright, D. B., Villarini, G., Paul, S., Kumar, D. N., Khedun, C. P., Niyogi, D., Schumann, G. & Stedinger, J. R. (2022) An overview of flood concepts, challenges, and future directions, *Journal of Hydrologic Engineering*, **27** (6), 1–30. https://doi.org/10.1061/(asce)he.1943-5584.0002164.

Nguyen, H. Q., Radhakrishnan, M., Huynh, T. T. N., Baino-Salingay, M. L., Ho, L. P., Steen, P. V. d. & Pathirana, A. (2017) Water quality dynamics of urban water bodies during flooding in Can Tho City, Vietnam, *Water*, **9** (4), 260. https://doi.org/10.3390/w9040260.

Olsson, G. (2019) Controlling urban drainage systems. In: Mannina, G. (ed.). *New Trends in Urban Drainage Modelling*. New York: Springer International Publishing, pp. 191–206.

Paulik, R., Chang-Ting, J. & Williams, S. (2025) Flood damage evaluation for buildings in a small island developing state, *Water Resources Research*, **61** (9), e2025WR040141. https://doi.org/10.1029/2025WR040141.

Pham Thi, H., Nghiem Quoc, D., Trinh Thi Hoai, T., Pham The, H. & Le Thi, N. (2019) Determination of the relationship between Vietnam national coordinate reference system (VN-2000) and ITRS, WGS84 and PZ-90, *E3S Web of Conferences*, **94**, 03014. https://doi.org/10.1051/e3sconf/20199403014.

Piadeh, F., Behzadian, K. & Alani, A. M. (2022) A critical review of real-time modelling of flood forecasting in urban drainage systems, *Journal of Hydrology*, **607**, 127476. https://doi.org/10.1016/j.jhydrol.2022.127476.

Pichler, M. (2025) Swmm_api: a Python package for automation, customization, and visualization in SWMM-based urban drainage modeling, *Water (Switzerland)*, **17** (9), 1373. https://doi.org/10.3390/w17091373.

Prokić, M., Savić, S. & Pavić, D. (2019) Pluvial flooding in urban areas across the European continent, *Geographica Pannonica*, **23** (4), 216–232. https://doi.org/10.5937/gp23-23508.

Qin, J., Gao, L., Lin, K. & Shen, P. (2024) A novel and efficient method for real-time simulating spatial and temporal evolution of coastal urban pluvial flood without drainage network, *Environmental Modelling and Software*, **172**, 105888. https://doi.org/10.1016/j.envsoft.2023.105888.

Qiu, Z., Wu, B., Chu, Q., Xie, X., Sun, R. & Jia, S. (2025) Spatiotemporal classification of short-duration heavy rainfall in Beijing using K-shape clustering, *Water (Switzerland)*, **17** (7), 968. https://doi.org/10.3390/w17070968.

Downloaded from iwaponline.com/hr/article-pdf/57/3/383/1608758/nh2026046.pdf
by Delft University of Technology user

Rogers, J. S., Maneta, M. P., Sain, S. R., Madaus, L. E. & Hacker, J. P. (2025) The role of climate and population change in global flood exposure and vulnerability, *Nature Communications*, **16** (1), 1287. https://doi.org/10.1038/s41467-025-56654-8.

Rosenzweig, B. R., McPhillips, L., Chang, H., Cheng, C., Welty, C., Matsler, M., Iwaniec, D. & Davidson, C. I. (2018) Pluvial flood risk and opportunities for resilience, *Wiley Interdisciplinary Reviews: Water*, **5** (6), 1–18. https://doi.org/10.1002/wat2.1302.

Sadkou, S., Artigue, G., Fréalle, N., Ayral, P., Pistre, S., Sauvagnargues, S. & Johannet, A. (2024) A review of flash-floods management: from hydrological modeling to crisis management, *Journal of Flood Risk Management*, **17**, e12999. https://doi.org/10.1111/jfr3.12999.

Sañudo, E., Cea, L., Puertas, J., Naves, J. & Anta, J. (2024) Large-scale physical facility and experimental dataset for the validation of urban drainage models, *Hydrological Processes*, **38** (1), 1–14. https://doi.org/10.1002/hyp.15068.

Schaum, S., Stenger-Wolf, S., Schüttrumpf, H. & Jüpner, R. (2025) An overview of long-term temporaries after flood disasters, *Journal of Flood Risk Management*, **18** (3), e70109. https://doi.org/10.1111/jfr3.70109.

Schmid, F. & Leandro, J. (2024) A data-driven multi-step flood inundation forecast system, *Forecasting*, **6** (3), 761–781. https://doi.org/10.3390/forecast6030039.

Seyoum, S. D., Vojinovic, Z., Price, R. K. & Weesakul, S. (2012) Coupled 1D and noninertia 2D flood inundation model for simulation of urban flooding, *Journal of Hydraulic Engineering*, **138** (1), 23–34. https://doi.org/10.1061/(ASCE)HY.1943-7900.0000485.

Shin, E., Kim, H.-J., Rhee, D. S., Eom, T. & Song, C. G. (2021) Spatiotemporal flood risk assessment of underground space considering flood intensity and escape route, *Natural Hazards*, **109** (2), 1539–1555. https://doi.org/10.1007/s11069-021-04888-2.

Snikitha, S., Kumar, G. P. & Dwarakish, G. S. (2025) A comprehensive review of cutting-edge flood modelling approaches for urban flood resilience enhancement, *Water Conservation Science and Engineering*, **10** (1), 2. https://doi.org/10.1007/s41101-024-00327-y.

Tanaka, T., Kiyohara, K. & Tachikawa, Y. (2020) Comparison of fluvial and pluvial flood risk curves in urban cities derived from a large ensemble climate simulation dataset: a case study in Nagoya, Japan, *Journal of Hydrology*, **584**, 124706. https://doi.org/10.1016/j.jhydrol.2020.124706.

Tellman, B., Sullivan, J. A., Kuhn, C., Kettner, A. J., Doyle, C. S., Brakenridge, G. R., Erickson, T. A. & Slayback, D. A. (2021) Satellite imaging reveals increased proportion of population exposed to floods, *Nature*, **596** (7870), 80–86. https://doi.org/10.1038/s41586-021-03695-w.

Tran-Anh, Q. & Ngo-Duc, T. (2024) Probabilistic projections of temperature and rainfall for climate risk assessment in Vietnam, *Journal of Water and Climate Change*, **15** (5), 2015–2032. https://doi.org/10.2166/wcc.2024.461.

Vasconcelos, J. G., Geller, V. G., Triboni, C. V., Wright, D. B. & Hodges, B. R. (2024) Evolution and characterization of pressurized flow conditions in stormwater collection networks, *Journal of Hydraulic Engineering*, **150** (2), 04024001. https://doi.org/10.1061/jhend8.hyeng-13835.

Vietnam Government (2006) *Nghị định về việc thành lập thành phố Hà Đông thuộc tỉnh Hà Tây - Decree of Establishing Ha Dong City, Ha Tay Province (155/2006/NĐ-CP)*. Vietnam: Vietnam Government.

Vietnam Government (2008) *Nghị định về việc điều chỉnh địa giới hành chính xã, phường, để thành lập phường thuộc thành phố Hà Đông, thành phố Sơn Tây, tỉnh Hà Tây – Decree of Adjusting Administrative Boundaries of Communes, Wards to Establish Wards in Ha Dong City and Son Tay City*. (23/2008/NĐ-CP). Vietnam: Vietnam Government.

Wang, L., Cui, S., Li, Y., Huang, H., Manandhar, B., Nitivattananon, V., Fang, X. & Huang, W. (2022) A review of the flood management: from flood control to flood resilience, *Heliyon*, **8** (11), e11763. https://doi.org/10.1016/j.heliyon.2022.e11763.

Wang, Y., Ye, Z., Jia, X., Liu, H., Zhou, G. & Wang, L. (2025) Flood disaster chain deduction based on cascading failures in urban critical infrastructure, *Reliability Engineering and System Safety*, **261**, 111160. https://doi.org/10.1016/j.ress.2025.111160.

Wijaya, O. T., Yang, T.-H., Hsu, H.-M. & Gourbesville, P. (2023) A rapid flood inundation model for urban flood analyses, *MethodsX*, **10**, 102202. https://doi.org/10.1016/j.mex.2023.102202.

Woo, H., Choi, H., Kim, M. & Noh, S. J. (2025) Physics-guided deep learning for spatiotemporal evolution of urban pluvial flooding, *Water (Switzerland)*, **17** (8), 1239. https://doi.org/10.3390/w17081239.

Yang, Q., Zheng, X., Jin, L., Lei, X., Shao, B. & Chen, Y. (2021) Research progress of urban floods under climate change and urbanization: a scientometric analysis, *Buildings*, **11** (12), 628.

Yen Nghia Comune People's Committee (2019) *The 2019 Viet Nam Population and Housing Census*. Confidential internal report.

Zeng, B., Huang, G. & Chen, W. (2025) Research progress and prospects of urban flooding simulation: from traditional numerical models to deep learning approaches, *Environmental Modelling and Software*, **183**, 106213. https://doi.org/10.1016/j.envsoft.2024.106213.

Zhou, Z., Smith, J. A., Baeck, M. L., Wright, D. B., Smith, B. K. & Liu, S. (2021) The impact of the spatiotemporal structure of rainfall on flood frequency over a small urban watershed: an approach coupling stochastic storm transposition and hydrologic modeling, *Hydrology and Earth System Sciences*, **25** (9), 4701–4717. https://doi.org/10.5194/hess-25-4701-2021.

Zhou, R., Zheng, H., Liu, Y., Xie, G. & Wan, W. (2022) Flood impacts on urban road connectivity in southern China, *Scientific Reports*, **12** (1), 1–17. https://doi.org/10.1038/s41598-022-20882-5.

Zhou, Y., Duan, Y., Yao, H., Li, X. & Li, S. (2025) Incorporating hydrological constraints with deep learning for streamflow prediction, *Expert Systems with Applications*, **259**, 125379. https://doi.org/10.1016/j.eswa.2024.125379.

Zhu, Z., Gou, L., Liu, S. & Peng, D. (2023) Effect of urban neighbourhood layout on the flood intrusion rate of residential buildings and associated risk for pedestrians, *Sustainable Cities and Society*, **92**, 104485. https://doi.org/10.1016/j.scs.2023.104485.

First received 19 March 2025; accepted in revised form 29 December 2025. Available online 19 January 2026

Downloaded from iwaponline.com/hr/article-pdf/57/3/383/1608758/nh2026046.pdf
by Delft University of Technology user